Cell Reports

Article

Apical Restriction of the Planar Cell Polarity Component VANGL in Pancreatic Ducts Is Required to Maintain Epithelial Integrity

Graphical Abstract

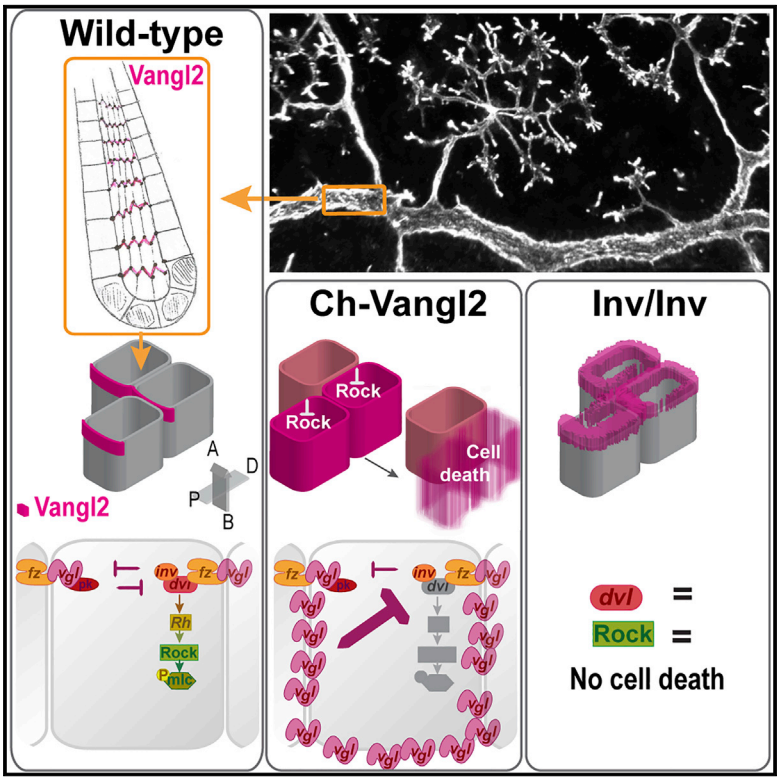

Highlights

- PCP components are restricted to apical junctions during pancreas development
- The core PCP protein VANGL is planar polarized along the duct
- Ectopic basolateral expansion of VANGL cell autonomously downregulates DVL and ROCK
- Decreased ROCK activity leads to cell egression, apoptosis, and pancreatic hypoplasia

Authors

Lydie Flasse, Siham Yennek, Cédric Cortijo, Irene Seijo Barandiaran, Marine R.-C. Kraus, Anne Grapin-Botton

Correspondence

flasse@mpi-cbg.de (L.F.), botton@mpi-cbg.de (A.G.-B.)

In Brief

Flasse et al. show that the PCP protein VANGL is polarized both along the apico-basal and planar axis in pancreatic ductal cells. VANGL apical restriction rather than its planar polarization is required for progenitor survival. This discriminates the importance of apical tethering of a PCP protein from its planar polarization.

Flasse et al., 2020, Cell Reports *31*, 107677
May 26, 2020
https://doi.org/10.1016/j.celrep.2020.107677

CellPress

Cell Reports

CellPress
OPEN ACCESS

Article

Apical Restriction of the Planar Cell Polarity Component VANGL in Pancreatic Ducts Is Required to Maintain Epithelial Integrity

Lydie Flasse,[1,3,*] Siham Yennek,[1] Cédric Cortijo,[2] Irene Seijo Barandiaran,[3] Marine R.-C. Kraus,[2] and Anne Grapin-Botton[1,3,4,*]

[1]The Novo Nordisk Foundation Center for Stem Cell Biology (DanStem), Faculty of Health Sciences, University of Copenhagen, 2200 Copenhagen, Denmark

[2]Swiss Institute for Experimental Cancer Research (ISREC), School of Life Sciences, Ecole Polytechnique Fédérale de Lausanne (EPFL), 1015 Lausannne, Switzerland

[3]Max Planck Institute of Molecular Cell Biology and Genetics, 01307 Dresden, Germany

[4]Lead Contact

*Correspondence: flasse@mpi-cbg.de (L.F.), botton@mpi-cbg.de (A.G.-B.)

https://doi.org/10.1016/j.celrep.2020.107677

SUMMARY

Cell polarity is essential for the architecture and function of numerous epithelial tissues. Here, we show that apical restriction of planar cell polarity (PCP) components is necessary for the maintenance of epithelial integrity. Using the mammalian pancreas as a model, we find that components of the core PCP pathway, such as the transmembrane protein Van Gogh-like (VANGL), become apically restricted over a period of several days. Expansion of VANGL localization to the basolateral membranes of progenitors leads to their death and disruption of the epithelial integrity. VANGL basolateral expansion does not affect apico-basal polarity but acts in the cells where Vangl is mislocalized by reducing Dishevelled and its downstream target ROCK. This reduction in ROCK activity culminates in progenitor cell egression, death, and eventually pancreatic hypoplasia. Thus, precise spatiotemporal modulation of VANGL-dependent PCP signaling is crucial for proper pancreatic morphogenesis.

INTRODUCTION

The establishment and maintenance of polarity are essential for the function of many cell types. In epithelia, two axes of polarity have been characterized: (1) apico-basal polarity orients cells from the free surface or the lumen to the basal lamina and (2) planar polarity coordinates the polarization of cell structures or behaviors in the plane of the tissue, orthogonal to the apico-basal axis (Butler and Wallingford, 2017; Campanale et al., 2017). Planar polarity coordinates the orientation of cell appendices, such as trichomes in fly wings or stereocilia bundles in the inner ear, directional cell movement, or the orientation of multicellular structures, such as mammalian hair (Goodrich and Strutt, 2011).

A key feature of planar polarity is the asymmetric localization of core molecules of the pathway along both the apical-basal polarity axis and the plane of the epithelium. An evolutionarily conserved core group of six families of proteins is required to coordinate planar polarization between neighboring cells: the transmembrane proteins Frizzled (vertebrate: FZD; fly: FZ), CELSR (CELSR; FMI), and Van Gogh-like (VANGL; STBM/VANG); and the cytosolic-submembrane proteins Dishevelled (DVL; DSH), Inversin/Diversin (INV/ANKRD6; DGO), and Prickle (PK). The planar cell polarity (PCP) signaling system uses intra- and intercellular feedback interactions between its core components to establish their characteristic asymmetric cellular distributions. In the most comprehensively characterized system, the *Drosophila* wing blade, the FZ-DSH-DGO complex localizes to intercellular junctions facing the VANG-PK complex in the adjacent cell. FMI, an atypical cadherin, localizes to both sides of the apical junction and bridges the FZ and VANG complexes between neighboring cells. These intercellular interactions are counterbalanced intracellularly by reciprocal inhibitory interactions between the two complexes (Goodrich and Strutt, 2011; Peng and Axelrod, 2012). VANGL, a component specific to the PCP, plays a central role in the establishment of the core protein complex (Hatakeyama et al., 2014). Mutations in the VANGLs underlie a broad spectrum of developmental disorders in humans (Butler and Wallingford, 2017), such as neural tube defects (Iliescu et al., 2014; Merello et al., 2015), renal (Papakrivopoulou et al., 2018; Schnell and Carroll, 2016), heart (Yuan et al., 2014; Li and Wang, 2018), and lung diseases (Yates and Dean, 2011). Moreover, recent studies have shown that VANGL2 is consistently upregulated and amplified in breast, ovarian, and uterine carcinomas (Hatakeyama et al., 2014), and a tumorigenic function has been established in rhabdomyosarcoma (Hayes et al., 2018).

The planar polarity components in *Drosophila* epithelia are anchored apically (Shimada et al., 2001; Strutt and Strutt, 2008), with this feature being conserved in the few vertebrate

organs investigated to date, as for example the inner ear (Montcouquiol et al., 2003, 2006; Butler and Wallingford, 2017). The principal regulators of epithelial apico-basal polarity include the apically localized Crumbs (Crb, PATJ, and Pals1) and Par complexes (Cdc42-Par6-aPKC) and the basolateral Scribble (Scrib, Lgl, and Dlg) complex. In addition, Par3 is commonly found at adherens junctions, whereas ZO-1 is a marker of the tight junction (Román-Fernández and Bryant, 2016).

Apico-basal and planar polarity are important for morphogenesis of organs comprising branched networks of tubules, such as the lungs, kidneys, and pancreas (Kunimoto et al., 2017). The developing pancreas consists of a network of tubes lined by polarized progenitors, the apical membranes of which line the duct lumen (Villasenor et al., 2010; Kesavan et al., 2009). This network is dynamic and remodeled throughout development with concomitant growth of the pancreatic epithelium and commitment of progenitors to specialized acinar, ductal, or endocrine (islet) cell fates (Dahl-Jensen et al., 2018). At embryonic day 10.5 (E10.5) in the mouse, multipotent progenitors are organized around discrete microlumens (Larsen and Grapin-Botton, 2017; Pan and Wright, 2011). By E12.5, these microlumens have fused to form a plexus of interconnected ducts. These ducts/primitive tubules are morphologically immature and are lined by duct-/endocrine-bipotent "trunk" progenitors that subsequently form mature duct cells while cells committing to the alternative endocrine lineage delaminate/egress and coalesce into islets. Progenitor cells at the "tips" of the network are initially multipotent (acinar, duct, and endocrine competent) and become progressively restricted to the acinar fate after E12.5, maturing during development and in the postnatal period (Larsen et al., 2017). By birth, the ducts are remodeled into an arborized structure (Dahl-Jensen et al., 2018; Bankaitis et al., 2015; Villasenor et al., 2010), which transports ductal secretions and acinar digestive enzymes to the duodenum. For the sake of convenience, we refer to all cells lining ducts/tubes as ductal cells, although their potency, structure, and functionality differ according to the temporal stages defined above.

We have previously shown that several PCP components are expressed in the embryonic pancreas and that inactivation of CELSR2/3 severely abrogates endocrine differentiation. Together, this suggests that PCP components are essential regulators linking pancreas morphogenesis with cell fate (Cortijo et al., 2012). In this study, we show that apical restriction of PCP components is gradual and that VANGL2 becomes planar polarized. By perturbing VANGL2 localization, we uncover that proper apical restriction of VANGL2 is required for the maintenance of epithelial integrity and progenitor survival.

RESULTS

Progressive Apical Restriction and Planar Polarization of PCP Components in the Tubular Epithelium of the Pancreas

We have previously shown that expression of VANGL1/2 is initiated in the pancreatic epithelium at around E11 when apico-basal polarity is first established (Cortijo et al., 2012). We observe that its cellular localization becomes progressively restricted to apical foci at cell junctions. A relatively long strip of staining observed at E14.5 along the apical-most third of the lateral membranes becomes restricted to punctate foci at E18.5 (Figures 1A–1C), in agreement with our previous quantifications at this stage (Cortijo et al., 2012). The VANGL1/2 domain does not extend to the apical membranes where Mucin1 is detected (Figures 1B and 1C). Although both FZD3 and FZD6 receptors can mediate PCP signaling (Wang et al., 2016) and both are transcriptionally expressed in the embryonic pancreas, we were only able to detect the FZD3 protein. Mirroring VANGL1/2 expression, small foci of the FZD3 protein were detected around emerging microlumens at E10.5 (Figure S1A). At E12.5, FZD3 was apically enriched in the branching epithelium, and although it is largely membrane restricted, some cytoplasmic signal was evident (Figure S1B). By E14.5, again paralleling VANGL1/2 expression, FZD3 was restricted to the apical-most third of the lateral membranes (Figures 1D and 1E) and, by E18.5, became condensed to foci at the apical cell junctions (Figure 1F). Both FZD3 and VANGL1/2 were expressed in distal tip and proximal trunk cells of the epithelium, with VANGL1/2 becoming enriched in the trunk at later stages (Figures 1A and 1D). Both were subsequently detected in endocrine islets of Langerhans at E18.5 (data not shown).

The transmembrane proteins VANGL1/2 and FZD3 can recruit PK and Dishevelled, respectively, to the membranes (Jenny et al., 2003; Axelrod, 2001; Bastock et al., 2003). We could detect both Prickle2 (PK2) and Dishevelled2 (DVL2) proteins in the pancreatic ducts. Like VANGL1/2 and FDZ3, PK2 is localized at the apical cell junction at E15.5 (Figures 1G and 1H). DVL2 is apically enriched in the developing ducts at E12.5 (Figure S1C) and E15.5 (Figures 1I–1K and S1D). However, DVL2 is not strictly restricted to the apical junction (Figures 1J and 1K) but also extends into the cortex below most of the apical membrane, forming wide rings from an apical perspective (Figure 1J) and continuous apical localization in cross-sections (Figure 1K), as opposed to the punctate foci of the other core PCP components examined (VANGL1/2: Figures 1B and 1C; FZ3: Figures 1E and 1F; and PK2: Figure 1H). Notably, high levels of DVL2 are detected in the cytoplasm of newly formed endocrine clusters (Figure 1I, arrows; Figure S1C, demarcated by dotted lines).

To determine whether PCP components are asymmetrically localized in the plane of the epithelium, we performed whole-mount staining on E18.5 pancreata, which allowed us to visualize the ducts in three dimensions (3D) (Figure 2A). In the large interlobular ducts, costaining for the apical and lateral membrane markers Mucin1 and β-Catenin, respectively, revealed ductal cells to be anisotropic, exhibiting elongated apical surfaces along the longitudinal axis of the ducts (Figures 2B–2D). VANGL1/2 was distributed asymmetrically in the apical plane, being enriched on the transverse membranes (perpendicular to the longitudinal axis of the duct), whereas it was almost absent on the longitudinal membranes (Figures 2B and 2D; Video S1). This asymmetric localization of VANGL1/2 indicates that this protein is polarized in the plane of the pancreatic ductal epithelium. We also observed an enrichment of the VANGL1/2 protein at tricellular junctions, "hot-spots" of epithelial tension (Higashi and Miller, 2017) (Figure 2C). In smaller ducts, the lumen is too narrow to enable the visualization of the apical plane. However, we observe a discontinuous staining for VANGL at the apical side, suggesting enrichment at tricellular junctions, as in larger ducts (Figures 2E and 2F).

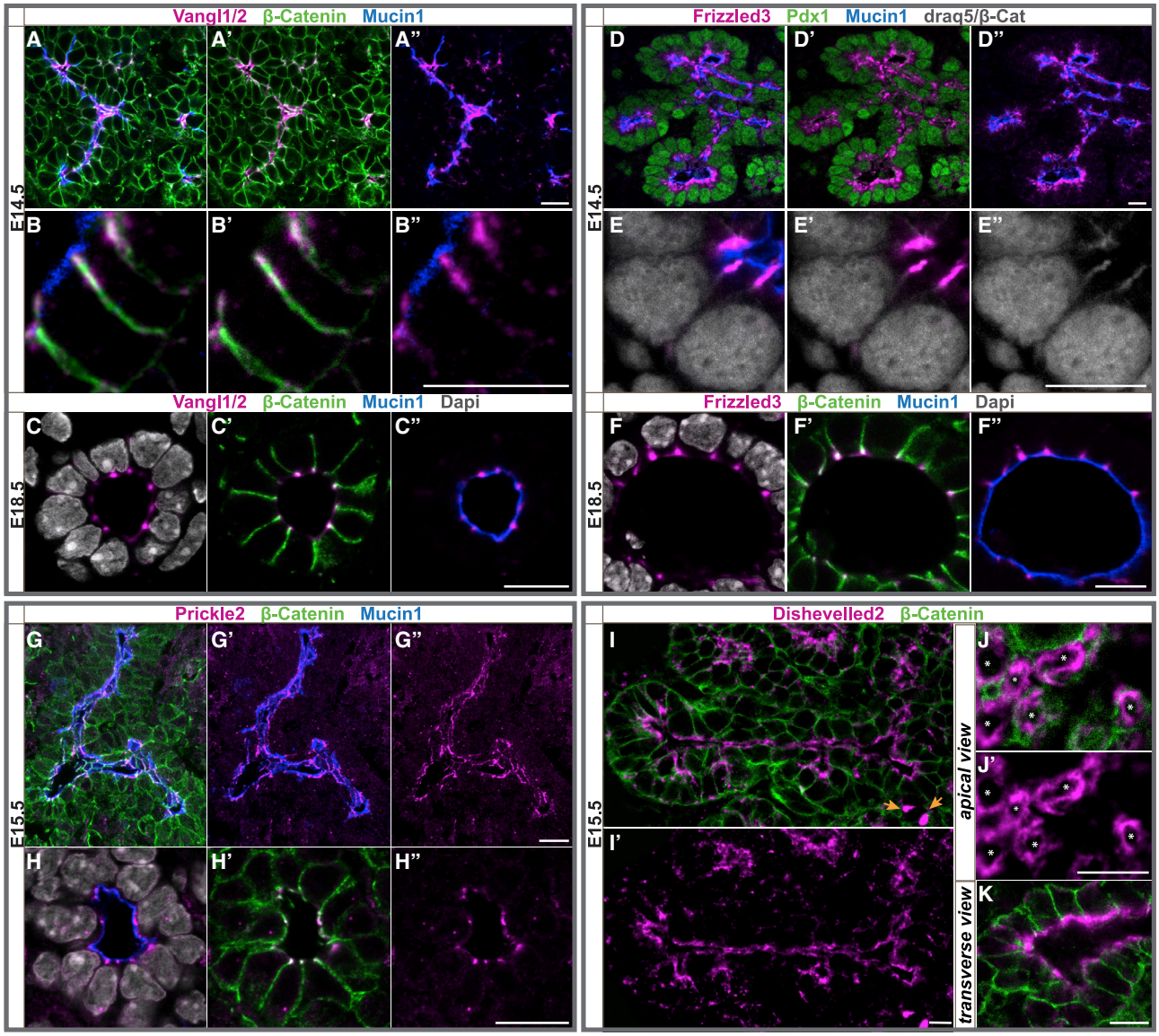

Figure 1. Apical Localization of PCP Components in the Pancreatic Epithelium

Confocal images (*z*-sections) of embryonic pancreas sections. β-Catenin and Mucin1 labels the basolateral and the apical membranes, respectively. PDX1 marks endocrine progenitors.

(A–F) At E14.5, VANGL and FZD3 are enriched at the apical side of the epithelium (A and D, respectively). Both proteins are located on the apical-most third of the lateral membrane (B and E). By E18.5, this domain is concentrated apically in foci located just below the apical membranes, where the cell junctions are positioned (C and F).

(G and H) PK2 is also located at apical cell junctions. Shown are (G) general view and (H) higher-magnification view.

(I–K) DVL2 is enriched apically in pancreatic epithelial cells (I) and in the cytoplasm of endocrine cells (I, orange arrows). In the epithelium, DVL2 is not restricted to the apical junction but lines the apical membrane (K). From an apical perspective, DVL2 forms rings at the apical cortex (J, each asterisk indicates one cell). Scale bar, 10 μm.

Analogous 3D expression analyses were attempted for the other PCP components, but despite extensive efforts, available antibodies proved to be incompatible with various whole-mount immunofluorescence protocols. Taken together, these analyses reveal that the transmembrane and membrane-associated proteins of the PCP pathway display progressive apical restriction in tubes as well as planar localization (VANGL).

Ectopic Localization of VANGL2 on Basolateral Membranes Leads to Cell Death and Pancreatic Hypoplasia

Although the importance of asymmetric localization of PCP proteins in the plane is well established in both *Drosophila* (Strutt et al., 2016) and vertebrates (Bailly et al., 2017), little is known in this respect regarding their apical restriction. To test the

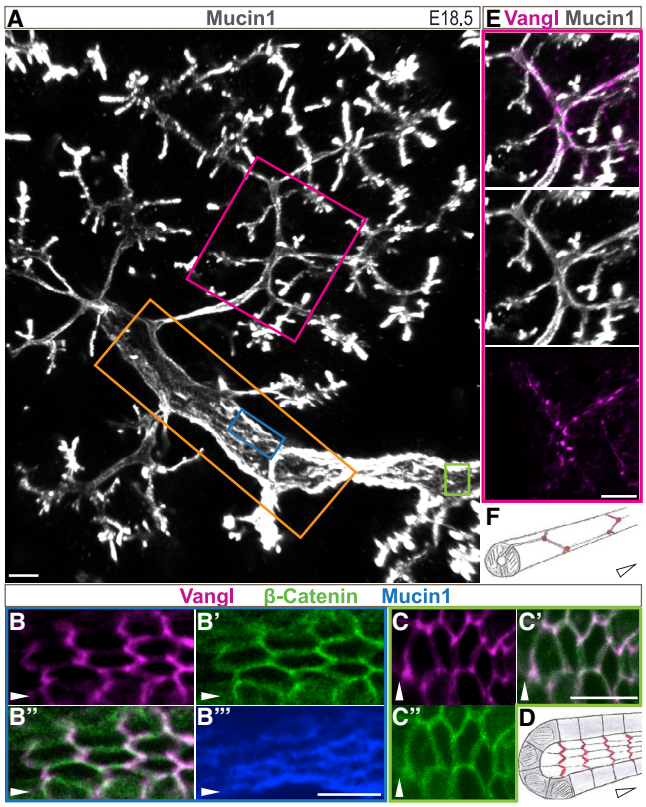

Figure 2. Planar Polarization of VANGL in the Tubular Epithelium of the Pancreas

(A) 3D projection of a whole-mount staining of Mucin1 depicting the architecture of the pancreatic ductal tree at E18.5. Rectangles delimit the area shown in Video S1 (orange), in (B) (blue), in (C) (green) and in (E) (magenta).

(B and C) Apical surface of cells in a large duct (confocal sections, arrowhead indicates the longitudinal axis of the duct). (B) Illustrates the asymmetric localization of VANGL on the transverse membranes. (C) Illustrates VANGL enrichment at the tricellular junctions.

(D) Scheme depicting VANGL (red) planar polarization in pancreatic duct.

(E and F) 3D projection of smaller ducts (E). The punctate pattern of VANGL suggests a similar planar distribution of the protein as represented in (F). Scale bar, 10 μm.

significance of VANGL2 expression and localization, we generated transgenic mouse lines in which Cre-mediated recombination inactivates β-actin promoter-driven GFP expression and induces expression of a Cherry-VANGL2 fusion protein (Figure 3A). This construct was previously reported to express a functional protein (Devenport and Fuchs, 2008). When expressed in pancreatic progenitors using *Pdx1*-Cre (Hingorani et al., 2003), the fusion protein was initially detected at the cell cortex in most pancreatic epithelial cells at E10.5 and, by E12.5, became membrane enriched (Figures S2A and S2B). Mesenchymal cells surrounding the epithelium expressed GFP, as expected from the nonrecombined transgene (Figure S2C). In contrast to endogenous VANGL proteins that are restricted to the apical junction in wild-type pancreata (Figure 3B), the Cherry-VANGL2 fusion protein was detected throughout the basal and lateral membrane surface (Figures 3C and 3D). Although this is a sizable expansion of the VANGL domain, we only detected a small increase of *Vangl2* transcript by qPCR at E14.5 (Figure S2D)

To determine whether ectopic VANGL localization throughout the cell membrane affects pancreas development, we analyzed pancreatic epithelial size in double-transgenic *Pdx1-Cre; Cherry-Vangl2* (*Ch-Vgl2*) mice versus control (single transgenic and wild type; see STAR Methods) littermates. At E10.5, when the Cherry-VANGL2 protein was first detectable in double-transgenic embryos, their pancreata were equivalent in size to controls (Figure S2E), but by E12.5, we observed a ~60% decrease in *Ch-Vgl2* pancreatic epithelial size (Figure 3E). Pancreatic hypoplasia in *Ch-Vgl2* embryos was maintained at E14.5 (Figures 3F and 3G) and was exacerbated at E16.5 (Figure S2F). At this stage, we observed an ~85% decrease in PDX1$^+$ progenitors and endocrine (glucagon$^+$ or insulin$^+$) cells (Figure S2F). Pancreatic hypoplasia was consistently observed in double-transgenic embryos generated from three independent lines of *Cherry-Vangl2* mice with various transgene expression levels (Figure S2G). Of note, for each line, we observed some variability in the recombination efficiency (proportion of Cherry$^+$ cells within the pancreatic epithelium) between individuals, likely accounting for the variability in pancreatic size evident between double-transgenic embryos (Figures 3E and S2E–S2G).

To test whether hypoplasia of Cherry-VANGL2-expressing pancreata resulted from reduced progenitor proliferation, we quantified the proportions of phospho-HistoneH3-expressing cells in the epithelium. No significant difference was detected between the proportions of proliferating epithelial progenitors in E12.5 *Ch-Vgl2* versus control siblings (Figures S2H–S2J). In contrast, TUNEL assays performed on E12.5 litters revealed only a few (0.07% on average) apoptotic cells in control pancreatic epithelia, whereas we observed a 2.2-fold increase in TUNEL$^+$ pancreatic epithelial cells in *Ch-Vgl2* littermates (Figure 3H). Moreover, the extent of hypoplasia positively correlated with the proportion of apoptotic cells (Pearson correlation test: $r = 0.8$; $p < 0.05$) (Figure S2K). In E12.5 *Ch-Vgl2* embryos, we also observed elevated numbers of TUNEL$^+$ cells among the mesenchymal cells located immediately adjacent to the epithelium (Figure 3H, arrows; Figure S2L). We propose that these cells, located at a distance of one or two cell diameters from the epithelium, are epithelial cells that have recombined and egressed from the distal-most epithelial layer. Staining for Cleaved Caspase-3 (Cas3) confirmed these observations, revealing an increased number of Cas3$^+$ cells in the epithelium expressing the Cherry-VANGL2 fusion protein (Figures 3I and 3J), some of which appeared to be egressing basally (Figure 3K). Furthermore, we detected dying (Cas3$^+$) cells retaining Cherry expression, indicating Cherry-VANGL2 expression can lead to cell death in the cells where it is mislocalized (Figure 3L). Concordantly, Annexin V staining on sorted pancreatic cells at E12.5 revealed the Cherry$^+$ population to be more apoptotic (Annexin V$^+$) than the nonrecombined (GFP$^+$) population (Figure 3M). Taken together, these findings show that ectopic basolateral membrane localization of the Cherry-VANGL2 protein in pancreatic epithelial cells leads to apoptosis of progenitors and, subsequently, to hypoplasia of the pancreas.

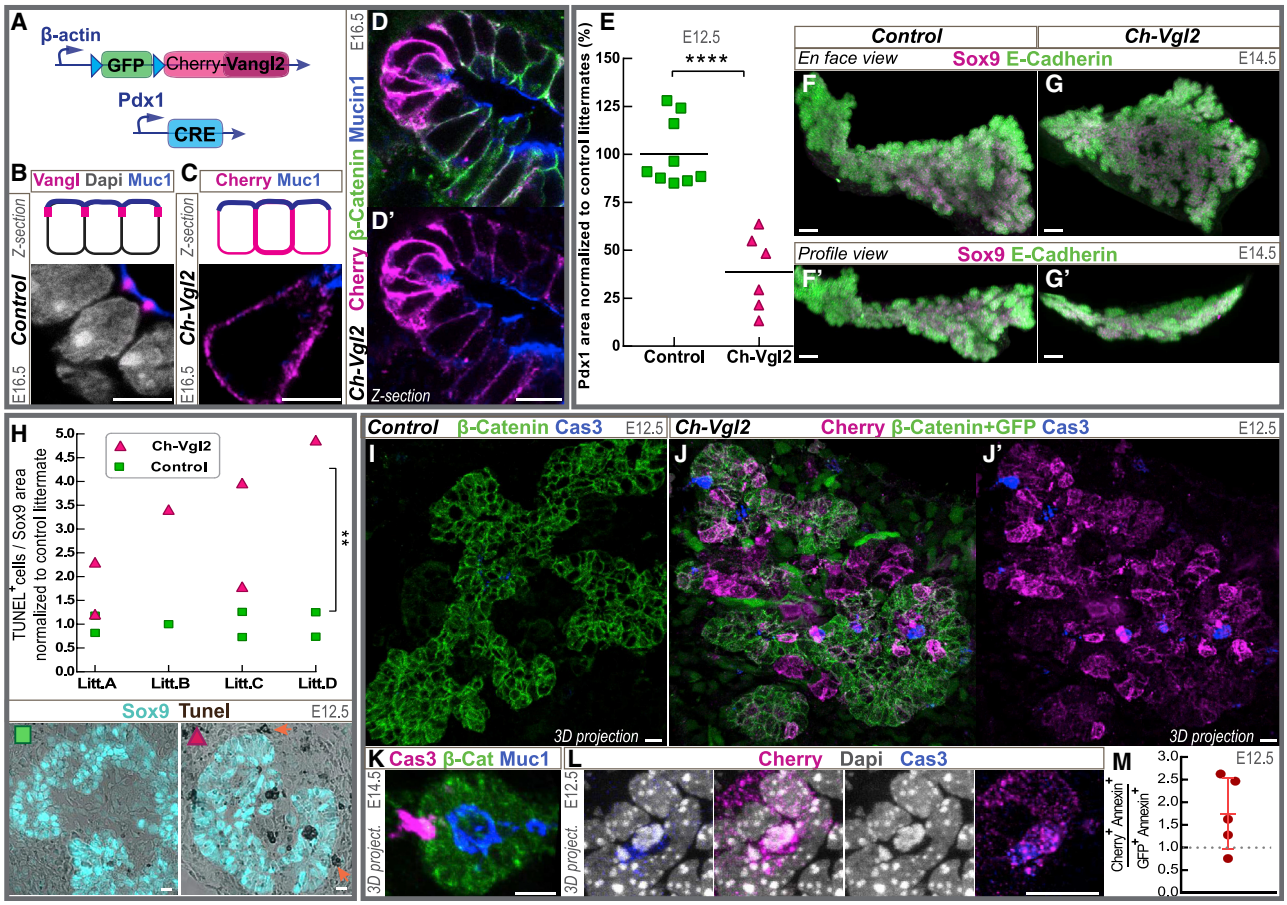

Figure 3. Ectopic Localization of VANGL2 on Basolateral Membranes Leads to Cell Death and Pancreatic Hypoplasia

(A) Schematic of the construct used to express the fusion protein Cherry-VANGL2 in pancreatic progenitors.

(B–D) Localization of VANGL in pancreatic section of control (*Pdx1-Cre Tg/+* or *Cherry-Vangl2 Tg/+* or wild-type) (B) and Cherry in *Ch-Vgl2* (*Pdx1-Cre Tg/+*; *Cherry-Vangl2 Tg/+*) (C and D).

(E) PDX1$^+$ area quantified on E12.5 pancreatic sections of control (green) and *Ch-Vgl2* (pink) show a decrease of epithelium size in *Ch-Vgl2* embryos. Each dot represents one pancreas. ****$p < 0.0001$ by t test.

(F and G) Whole-mount immunostaining of SOX9 (progenitors) and E-cadherin (epithelial membranes) in *Ch-Vgl2* (G) and control littermate (F).

(H) TUNEL assay labeling apoptotic cells in pancreatic epithelium (SOX9$^+$) sections show an increase of cell death in *Ch-Vgl2*. Data are presented by litter, and each dot represents one pancreas. **$p = 0.004$ by t test. The orange arrows indicate dead cells that egressed the epithelial layer.

(I–L) Cleaved Caspase-3 (Cas3) immunostaining on sections showing dying cells in Cherry$^+$ regions (I and J). Close up in (L) shows one dying cell (Cas3$^+$ and with fragmented nuclei) expressing Cherry-VANGL2 protein. (K) Whole-mount immunostaining showing egression of a Cas3$^+$ cell.

(M) Annexin V staining on sorted pancreatic cells. The proportion of dying cell in the Cherry$^+$ population relative to the one in the GFP$^+$ cells is plotted on the y axis. Scale bar, 5 μm (B and C); 10 μm (D and B–L); 50 μm (F and G).

Loss of Epithelial Integrity upon Ectopic VANGL Localization

To further investigate how ectopic VANGL affects epithelial integrity, we conducted live imaging of pancreatospheres. These structures comprise a spherical monolayered pancreatic progenitor epithelium and are, thus, simpler than the branched pancreatic epithelium and more amenable to observation of epithelial structure in live imaging (Greggio et al., 2013; Sugiyama et al., 2013). Pancreatospheres were generated from *Ch-Vgl2* and control littermate pancreatic epithelia at E13.5. We consistently observed a disruption of the epithelia of pancreatospheres originating from *Ch-Vgl2* pancreata (Figure S3; Videos S2, S3, S4, S5, and S6). The wild-type or control (*Cherry-Vangl2* Tg/+; *Pdx1-Cre* +/+) pancreatospheres present a smooth monolayered epithelium lining and lumen (Figure S3A) of constant size in 3- and 5-h-long videos (Videos S2 and S3, respectively). In contrast, the epithelia of *Ch-Vgl2* pancreatospheres exhibit local multilayered thickenings (Figures S3B′ and S3F) and cell egression (Figures S3C) with eventual lumen collapse (Figures S3B′′ and S3D; Videos S2 and S4 compared as well as Videos S5 and S6 compared to Video S3). To test whether apoptosis occurred in spheres expressing the Cherry-VANGL2 fusion protein as it does *in vivo*, we performed a 30-min pulse with DAPI on the growing spheres to label dead cells (Figures S3E and S3F). Postpulse imaging revealed an average of 1.3% dead cells with condensed DAPI$^+$ nuclei in controls

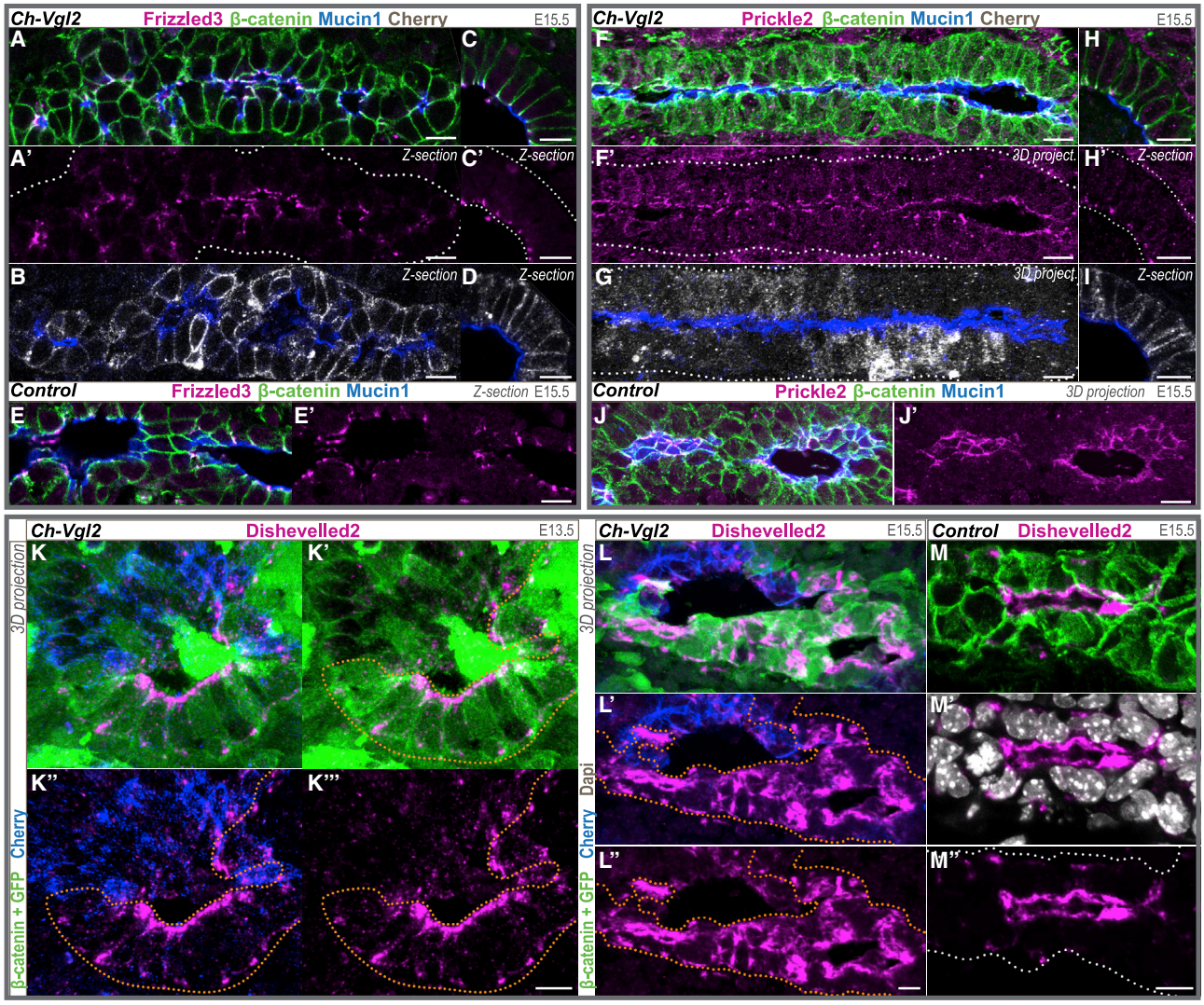

Figure 4. Ectopic VANGL Localization Perturbs Dishevelled but Not Prickle nor Frizzled Localization

Immunostaining on pancreatic sections showing the localization of PCP components. Longitudinal (A, B, E–G and J) and transverse (C, D, H, I, and K–M) sections of ducts.

(A–E) Frizzled3 is expressed at the apical cell junctions in Cherry-VANGL2^{+} regions (A–D) as in the control (E). Sections (B) and (D) are adjacent to (A) and (C), respectively.

(F–J) Prickle2 is expressed at the apical cell junction in the Cherry-VANGL2^{+} regions (F–I), as in the controls (J) (Figure 1H). Sections (F) and (H) are adjacent to (G) and (I), respectively.

(K–M) At E13.5 (K) and E15.5 (L) Dishevelled2 (magenta) expression is decreased in the Cherry^{+} cells (blue) compared to the adjacent cells not expressing the Cherry-VANGL2 protein (GFP^{+} cells; green and demarcated by orange dotted lines) or the unrecombined cells (M). Scale bar, 10 μm.

and an 8.3-fold increase in *Ch-Vgl2* pancreatospheres (Figure S3G). Taken together, our *in vivo* and *ex vivo* data show that ectopic mislocalization of VANGL to the basolateral membrane leads to loss of epithelial integrity, cell egression, and cell death.

Ectopic VANGL Localization Does Not Perturb Apico-basal Polarity but Interferes with Dishevelled Localization

As defects in apico-basal polarity have previously been associated with apoptosis (Knust et al., 1993; Kolahgar et al., 2011; Müller and Wieschaus, 1996; Tepass et al., 1990), we tested whether expansion of the VANGL domain to the basolateral membrane impacts apico-basal marker localization. Indeed, although VANGL is mainly known to regulate PCP, previous reports have intimated at a role for VANGL2 in maintaining apico-basal polarity (Lindqvist et al., 2010; Tao et al., 2009; Vandenberg and Sassoon, 2009; Hatakeyama et al., 2014; Milgrom-Hoffman and Humbert, 2018). The cellular localization of the apical membrane glycoprotein Mucin1 (Figures 4A–4J), the apical junction marker PAR3 (Figures S4A–S4E), the tight junction protein ZO-1 (Figures S4A–S4E), the basolateral marker Scribble

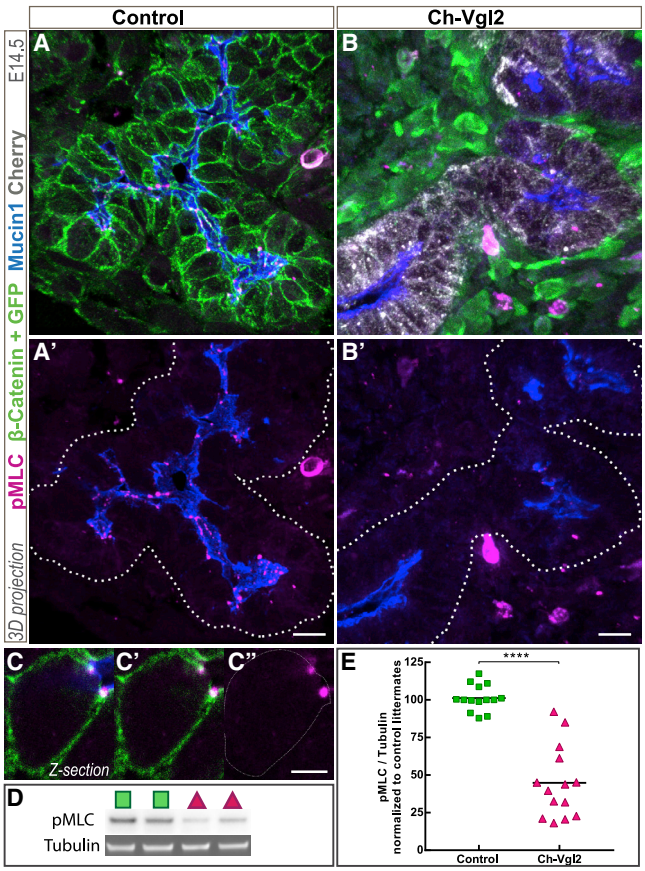

Figure 5. Decreased Actomyosin Contractility upon Mislocalization of VANGL

(A and B) Pancreas section immunostained for pMLC. Note the disappearance of pMLC$^+$ apical foci in the *Ch-Vgl2* section (B) compared to control littermate (A).

(C) Close-up highlighting the localization of pMLC at the apical cell junction in a control sample.

(D) Representative image of the pMLC western blots used for the quantification in (E).

(E) Decrease of pMLC level in *Ch-Vgl2* samples compared to the control. Each dot corresponds to one pancreas.

****$p < 0.0001$ by t test. Scale bar, 5 μm (C); 10 μm (A and B).

(Figures S4A–S4E), and the apical marker αPKC (Figures S4F–S4K) were all unaffected in Cherry-VANGL2-expressing cells, strongly indicating that the integrity of the apico-basal axis is conserved in *Ch-Vgl2* pancreata.

VANGL physically interacts with the majority of the other PCP components (Bailly et al., 2017), and depending on the context, manipulation of VANGL localization can affect the level and/or localization of these proteins. Hence, we systematically examined the localization of VANGL2 partners in our basolateral VANGL2 mislocalization model. Frizzled and VANGL interact across the membranes of adjacent cells (Wu and Mlodzik, 2008), bridged by the atypical cadherin CELSR, enabling the propagation of polarity from cell to cell (Strutt and Strutt, 2007). In *Ch-Vgl2* pancreata, Frizzled3 localization and apparent level were unaffected (Figures 4A–4E). Thus, VANGL basolateral expansion fails to induce a similar expansion of the Frizzled3 domain.

Intracellularly, PK directly binds to VANGL and can bind to Dishevelled to antagonize its Frizzled-mediated membrane recruitment (Bastock et al., 2003; Carreira-Barbosa et al., 2003; Jenny et al., 2003; Tree et al., 2002). However, in *Ch-Vgl2* pancreata, we did not detect any changes in the localization of PK2 at E13.5 or E15.5 (Figures 4F–4J; data not shown).

Dishevelled can be physically bound by VANG in *Drosophila*, and in vertebrates, these interactions are believed to antagonize the formation of the FZD-DVL complex by affecting DSH/DVL levels and/or stability (Yang and Mlodzik, 2015; Bastock et al., 2003; Park and Moon, 2002; Seo et al., 2017). In *Ch-Vgl2* pancreata at E13.5 and E15.5, we observed a decrease in DVL2 levels in the cells expressing Cherry-VANGL2 protein (Figures 4K–4M; Figure S4L). In the adjacent cells that were not expressing the fusion protein, the level and localization of DVL2 remain unchanged (Figures 4K–4M; Figure S4L), suggesting that ectopic localization of VANGL2 perturbs the level and/or stability of DVL2 in a cell autonomous manner.

Decreased Actomyosin Contractility upon VANGL Mislocalization

Actomyosin contraction, mediated by activation of Rho kinase, is well-recognized as an important downstream effector of DVL (Habas et al., 2001; Nishimura et al., 2012; Park et al., 2005). Moreover, VANGL itself has also been implicated to play a role in remodeling of actin microfilaments (Chen et al., 2016; Galea et al., 2018; Lindqvist et al., 2010; McGreevy et al., 2015; López-Escobar et al., 2018). Furthermore, actomyosin contractility is associated with apoptosis in different contexts (Ohsawa et al., 2018). For these reasons, we examined phosphorylation of myosin regulatory light chain (pMLC), a substrate of Rho kinase and effector/readout of actomyosin-based contraction (Vicente-Manzanares et al., 2009) in *Ch-Vgl2* pancreata. Immunostaining showed pMLC to be apically polarized in E12.5 control pancreata, whereas the protein was undetectable in *Ch-Vgl2* pancreatic epithelia (Figures S5A and S5B). At E14.5, pMLC was expressed at the apical cell junction in controls (Figures 5A and 5C), mirroring the distribution of core PCP components, but pMLC was almost undetectable in Cherry-VANGL2-expressing epithelia (Figure 5B). Western blotting on E12.5 (Figure S5C) and E14.5 (Figures 5D and 5E) dorsal pancreata confirmed these observations, revealing a 60% decrease in average pMLC levels in pancreata from E14.5 *Ch-Vgl2* embryos compared with control siblings (Figure 5E). Taken together, these results indicate decreased ROCK pathway activity to be associated with VANGL basolateral mislocalization.

Jun N-terminal Kinase (JNK) has also been reported as a downstream effector of DVL (Boutros et al., 1998; Li et al., 1999; Moriguchi et al., 1999), although its function downstream of the core components—especially VANGL—remains unclear (Lapébie et al., 2011). Western blotting for phospho-c-*jun* did not reveal any significant dysregulation of JNK pathway activity in E14.5 *Ch-Vgl2* compared with control pancreata (Figures S5D and S5E). This suggests that the mechanism of VANGL-mislocalization-induced cell death is independent of the JNK pathway.

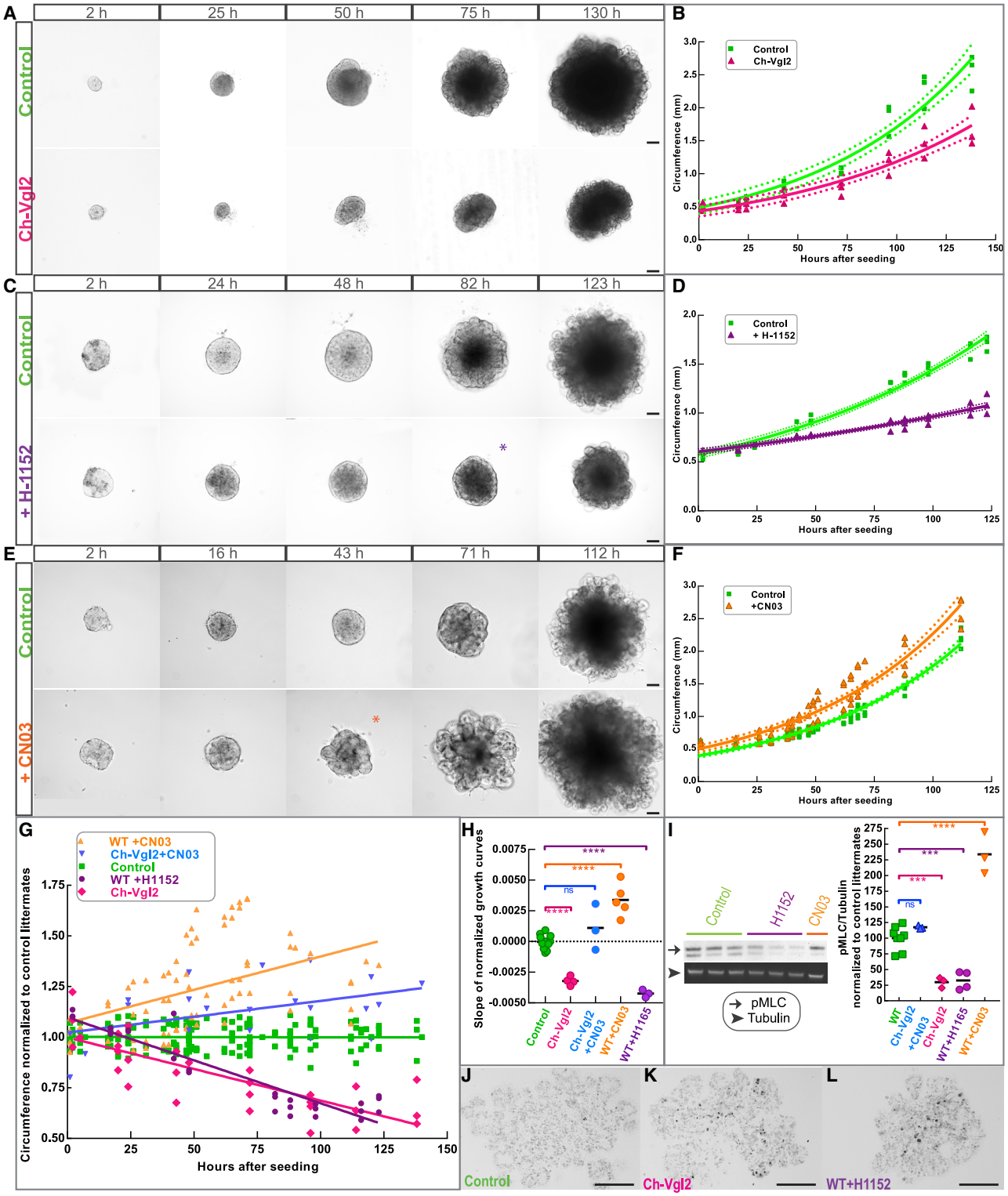

Figure 6. Activation of the RhoA Pathway Rescues Cell Death and Hypoplasia Induced by Ectopic VANGL Localization

(A–F) Culture in 3D Matrigel of E10.5 pancreatic epithelia from wild-type (WT) or *Ch-Vgl2* embryos treated with ROCK inhibitor (H-1152) or RhoA activator (CNO3). (A, C, and E) Images of the growing epithelium in each experimental condition at stated time points of culture (h, hours postseeding). (B, D, and F) Quantification of epithelial growth curve show that *Ch-Vgl2* (pink in B) and WT buds treated with ROCK inhibitor (purple in D) grow slower than those of their WT littermates (green); p = 0.01 and 0.006, respectively (t test, n = 3 in each condition). The WT buds treated with RhoA activator (orange in F) behave as controls (green; p = 0.8, n = 3).

(legend continued on next page)

RhoA Pathway Activation Rescues the Cell Death and Pancreatic Hypoplasia Induced by VANGL Basolateral Mislocalization

Taken together, our analyses reveal increased cell death and reduced ROCK pathway activity following VANGL membrane mislocalization. In order to determine whether elevated apoptosis in *Ch-Vgl2* pancreata is attributable to decreased ROCK pathway activity, we tested whether pharmacological activation of the ROCK pathway in *Ch-Vgl2* pancreatic epithelium is sufficient to rescue apoptosis and the resultant organ hypoplasia. To manipulate the ROCK pathway conveniently, we used an *ex vivo* culture system similar to our previously published pancreatic organoid model (Greggio et al., 2013) but in which the whole E10.5 pancreatic epithelium is seeded in Matrigel, enabling 3D growth in the absence of mesenchyme. The growth of the developing pancreas was evaluated daily by measuring the circumference of the epithelial bud. The pancreatic buds expressing Cherry-VANGL2 grew more slowly and remained smaller than those from control littermates at the end of the 5-day culture period, recapitulating the phenotype observed *in vivo* (Figures 6A and 6B). Inactivation of ROCK activity (via H1152, 5 μM) in wild-type epithelium manifested in an almost indistinguishable phenotype from the one observed for the *Ch-Vgl2* buds (Figures 6C and 6D). Of note, we also observed a delay in branching of the pancreatic epithelium when the ROCK pathway was inhibited (Figure 6C, asterisk). On the contrary, wild-type buds treated with a RhoA activator (CN03, 1 μg/μl) became bigger and branched precociously compared with control vehicle-treated buds (Figures 6E and 6F). Finally, activation of RhoA in *Ch-Vgl2* pancreatic epithelium rescued the hypoplasia (Figures 6G and 6H, normalized data; for details, see STAR Methods). In order to assess the level of ROCK pathway activity resulting from the various perturbations above, we performed western blotting for pMLC on treated individual buds (Figure 6I). The amount of pMLC protein was decreased by ~70% in untreated *Ch-Vgl2* buds (70% ± 4%) and wild-type buds treated with ROCK inhibitor (68% ± 7%), whereas in *Ch-Vgl2* buds treated with RhoA activator, pMLC levels were comparable to controls, indicating that ROCK pathway activity was restored to endogenous levels (Figure 6I). Lastly, we observed that *Ch-Vgl2* buds as well as wild-type buds treated with the ROCK inhibitor H1152 exhibited extensive apoptosis (Figures 6J–6L). In combination, these rescue experiments strongly indicate that the pancreatic hypoplasia resulting from VANGL2 mislocalization is significantly attributable to decreased ROCK pathway activity inducing apoptosis of progenitors.

Apical VANGL Accumulation Leads to Loss of Planar Asymmetry but Neither Induce Cell Death nor Perturb Actomyosin Contractility

We sought to distinguish whether cell death and epithelial exit in *Ch-Vgl2* pancreata resulted from ectopic localization of VANGL on the basolateral membrane or overexpression of the protein in general. To this end, we exploited an observation we made in another context, namely that *Inversin* mutants ($Invs^{Inv/Inv}$) (Morgan et al., 1998; Simons et al., 2005; Yokoyama et al., 1993) exhibit increased VANGL protein expression at the apical side of pancreatic ducts (Figures 7A–7G). In these mutants, in contrast to our observations in *Ch-Vgl2* pancreata, the localization of VANGL did not extend to the basolateral membrane but was increased at apical junctions and expanded within the apical membrane domain (Figures 7B and 7D). Whole-mount staining on E17.5 $Invs^{Inv/Inv}$ pancreata and en face apical views revealed a loss of VANGL planar asymmetric patterns (Figures 7E–7H).

This model of apical mislocalization of VANGL without lateral expansion does not display any defect in the size of the pancreas at E12.5 or E14.5 (Figure S6A) nor increased apoptosis (Figures S6B–S6D). Moreover, the level and localization of pMLC were unchanged in $Invs^{Inv/Inv}$ mutant pancreata relative to controls (Figures S6E–S6G), suggesting that ROCK pathway activity is unaffected. Finally, DVL2 protein expression levels and localization were also unaffected in the $Invs^{Inv/Inv}$ pancreatic epithelium (Figures S6H and S6I).

Although it may be argued that inversin mutation may exert effects on other proteins, these findings show that increasing the level of VANGL at the apical junction and/or loss of planar distribution of VANGL is not sufficient in itself to invoke cell death and epithelial disruption. This strongly suggests that in the *Ch-Vgl2* model it is the basolateral expansion rather than apical mislocalization of VANGL that induces cell death and epithelial disruption (Figure 7J).

Misexpression of VANGL2 Protein in the Neural Tube Also Induces Apoptosis

In order to ascertain whether the effects of VANGL mislocalization are pancreas specific or common across various epithelial paradigms, we induced the expression of Cherry-VANGL2 protein in the neural tube by using the $Rosa26^{CreER}$ driver. VANGL protein is apically polarized in this tissue and plays an essential role in neural tube closure and elongation (Torban et al., 2012). Induction of the transgene was performed at E11 by injection of 4OH-tamoxifen into the pregnant females, and embryos were harvested at either 6, 14, 24, or 48 h postinjection. Staining for Cleaved Caspase-3 revealed

The t test on the size of the bud at the end of the culture period shows that the *Ch-Vgl2* buds and the WT buds treated with ROCK inhibitor are smaller ($p = 0.02$ and 0.001, respectively), whereas the WT buds treated with the activator became larger ($p = 0.02$).

(G) Normalization of all the growth curves to the control littermates (see STAR Methods), showing that activation of the ROCK pathway in *Ch-Vgl2* buds can rescue the hypoplasia phenotype.

(H) Statistical analysis performed on the slope of the normalized data presented in (G). Each dot represents the growth of one bud; colors indicate the different experimental conditions; ****$p < 0.0001$; ns, nonsignificant.

(I) Western blot for pMLC and quantification of the band intensities. One dot represents the pMLC/Tubulin ratio for an individual bud. ****$p < 0.0001$; ***$p \leq 0.0005$; ns, nonsignificant.

(J–L) TUNEL assay on bud sections shows an increase of apoptosis in the *Ch-Vgl2* buds (K) as well as in the WT buds treated with ROCK inhibitor (L) compared to the control sibling (J). Scale bar, 100 μm.

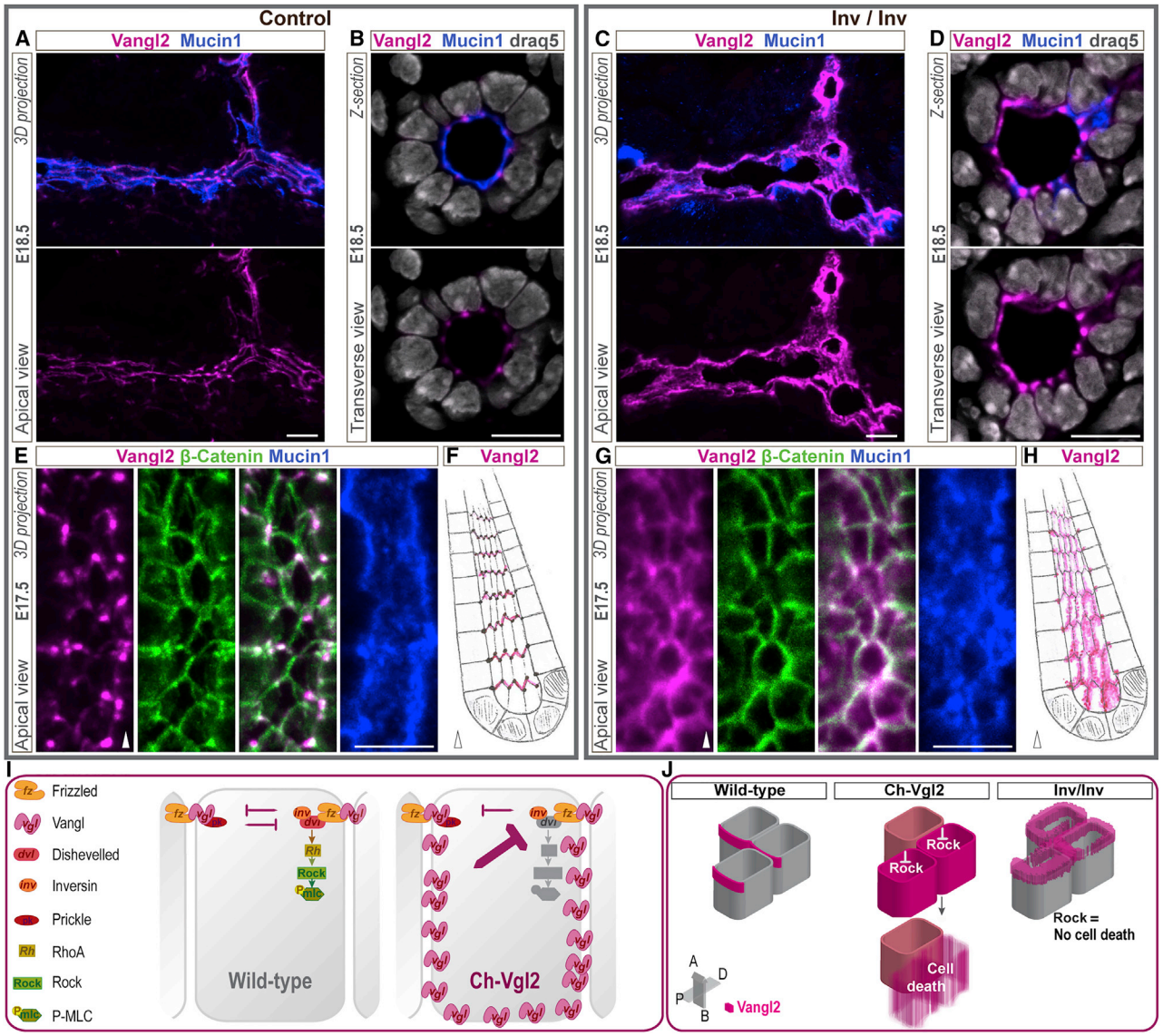

Figure 7. Increased Apical Levels of VANGL in the *inversin* Mutant Induce a Loss of Planar Asymmetry

(A–D) Pancreas section immunostained for VANGL shows an increase of the protein at the apical membrane in the *inversin* mutant (C and D) compared to the WT littermate (A and B).

(E–H) Whole-mount staining for VANGL showing the apical surface of ductal cells in *inversin* mutant (G) and control littermate (E); the arrowheads indicate the longitudinal axis of the duct. (F) Schematic of the planar-polarized organization and tricellular enrichment of VANGL in controls, while (H) shows the perturbation of this organization in the *inversin* mutant.

(I) Working model: in WT cells (left), VANGL is restricted to the apical junctions and the ROCK pathway is activated downstream of the FZD/DVL complex. In the *Ch-Vgl2* (right), VANGL is extended to the basolateral membranes. The FZD3 and PK2 are unchanged, whereas DVL level and ROCK pathway activity are decreased at the apical junction. We propose that basolateral expansion of VANGL leads to a cell-autonomous decrease of DVL protein and, consequently, of the downstream ROCK activity.

(J) Results summary: in the WT, VANGL is asymmetrically distributed at the apical side of the duct. In the *Ch-Vgl2* pancreas, VANGL extends all around the cell on the basolateral membranes that leads to a decrease of actomyosin contractility (detailed in I) and eventually to cell death. In the *inversin* mutant, apical levels of VANGL are increased, but no cell death or perturbation of actomyosin contractility is detected. In this mutant, planar asymmetry of the protein is also lost, suggesting that it is the basolateral expansion of VANGL rather than its apical mislocalization that induces cell death in the *Ch-Vgl2* pancreas. Scale bar, 10 μm.

a significant 3.3-fold increase in the proportion of apoptotic cells within the neural epithelium following the induction of the transgene, peaking at 14 h postinjection (Figure S7). Therefore, we can conclude that VANGL mislocalization induces apoptosis not only in the developing pancreatic epithelium but also in diverse epithelial organs.

DISCUSSION

In this study, we demonstrate that the proper localization of the PCP core component VANGL at the apical cell junction is required for the survival of pancreatic progenitors and, hence, for normal pancreatic morphogenesis. This apical localization is also necessary for cell survival in a structurally distinct epithelium, namely, the neural tube. Using transgenic lines driving the mislocalization of Cherry-VANGL2 protein throughout the whole basolateral membrane of pancreatic progenitors, we show that ectopic localization of this protein in the basolateral domain leads to apoptosis by downregulation of the ROCK pathway. Live imaging of pancreatospheres revealed this phenomenon to be associated with a disruption of epithelial integrity. Moreover, systematic analyses of the localization of core PCP components allowed us to decipher a mechanism of intracellular inhibitory interactions of possible relevance to other organs. We propose a model whereby expansion of VANGL localization—from its normally restricted position at the apical junctional contacts between cells—to the basolateral domain increases the previously reported (Kolahgar et al., 2011; Vandenberg and Sassoon, 2009) cell-autonomous repression exerted on Dishevelled, hence preventing its localization at the apical membrane (Figure 7I). The unchanged localization and expression level of FZD3 suggests that VANGL perturbations in a cell are not propagated to adjacent cells and, accordingly, that apoptosis is predominantly restricted to cells exhibiting VANGL mislocalization. As VANGL can bind Dishevelled in the fly (Bastock et al., 2003) as well as in vertebrates (Park and Moon, 2002), VANGL may directly destabilize DVL and inhibit its recruitment to the junctions by FZD. This hypothesis is strongly supported by findings from the Tomlin lab in *Drosophila* showing the ability of VANG to cell-autonomously block recruitment of DSH at the membrane (Amonlirdviman et al., 2005), resembling the previously reported repression of DSH by PK (Amonlirdviman et al., 2005; Jenny et al., 2003; Tree et al., 2002). However, in our system, mislocalization of VANGL protein does not induce a parallel expansion of its interaction partner PK. PK is, therefore, unlikely to contribute to the repression exerted on DVL. Recruitment of Dishevelled at the membrane is essential for its function in PCP (Axelrod, 1998, 2001). More specifically, its membrane localization in *Xenopus* gastrulating cells is required for activation of Rho and Rac (Park et al., 2005), the small GTPases active downstream of the Frizzled-Dishevelled module. Our results corroborate these data in mammals as we show a decrease of ROCK activity in Dishevelled^{low} (Cherry^{+}) cells. Precisely how VANGL perturbs DVL level/stability remains unclear but one possibility is ubiquitin-mediated degradation, a mechanism recently proposed to modulate PCP protein levels (Narimatsu et al., 2009; Strutt et al., 2013). In particular, VANGL1/2 promotes NRDP1-mediated Dishevelled ubiquitination in cell lines (Wald et al., 2017). Interestingly, in the *Inversin* mutant, which exhibits an upregulation of VANGL protein exclusively at the apical domain, such a downregulation of Dishevelled protein is not observed. Likewise, the increased cell death, epithelium integrity defects, and ROCK activity dysregulation of *Ch-Vangl2* pancreata were not recapitulated in *Inversin* mutants. However, because planar polarity is perturbed in both *Ch-Vgl2* and *Inversin* mutants, we conclude that the ectopic localization of VANGL on the basolateral membrane, rather than its increased level or apical expansion, is the key factor responsible for this phenotype and that robust restriction of VANGL protein activity to the apical junctions is essential for cell survival.

Interactions between apico-basal polarity and planar polarity have been reported (Apodaca, 2018; Butler and Wallingford, 2017; Djiane et al., 2005), but to date, only apico-basal polarity defects have been linked to apoptosis. In the fly, it is well established that disruption of apico-basal components, such as crumbs, stardust, or bazooka, lead to apoptosis (Knust et al., 1993; Müller and Wieschaus, 1996; Tepass et al., 1990). Our work reveals that disrupted apico-basal expression of a *PCP* core component can also manifest in cell death. The downstream pathways involved differ, as the in fly, activation of the JNK pathway triggers apoptosis (Kolahgar et al., 2011), whereas we show here that decreased ROCK pathway activity induces apoptosis following ectopic localization of VANGL. ROCK signaling can serve as either a proapoptotic or prosurvival cue in a cell-type- and context-dependent manner (Street and Bryan, 2011). In particular, in human airway epithelial cells, ROCK inhibition induces apoptosis by activation of the caspase cascade (Moore et al., 2004). Our studies suggest that this mechanism is conserved in the pancreatic epithelium. We also show that Cherry-VANGL2-positive cells are predisposed to undergo apoptosis and exit from the epithelium, suggesting that ectopic VANGL localization promotes egression in a cell-autonomous manner. The causal relationships between actomyosin dynamics, egression, and cell death have been debated in recent investigations (Ohsawa et al., 2018). Hence, one hypothesis is that mosaic transgene expression results in various levels of actomyosin activity between cells, leading cells with low actomyosin activity to be excluded by neighboring cells exerting higher tension before or after cell death. Such mosaic patterns are reminiscent of cell competition processes observed in apico-basal polarity-deficient clones. In both fly and MDCK cells, cells lacking basolateral determinants, such as Scribble, Mahjong, and Lethal giant larvae, undergo apoptosis if wild-type cells surround them (Di Gregorio et al., 2016). Interestingly, Scribble-deficient clones are also eliminated by extrusion and, ultimately, apoptosis (Vaughen and Igaki, 2016; Norman et al., 2012). These competition mechanisms that eliminate abnormal cells are essential for preventing tumor development and such a mechanism may be at play in the case of aberrantly VANGL-polarized cells. Van Gogh-like proteins are upregulated in many types of aggressive cancers, and this upregulation is associated with poor patient prognosis in breast cancer (Saito et al., 2018; VanderVorst et al., 2018; Daulat and Borg, 2017).

In addition, our study clarifies the spatial organization of the PCP in the pancreas. Using whole-mount staining enabled us to visualize tubes in three dimensions and to uncover how the PCP protein VANGL is organized, looking from inside the tube lumen to the apical surfaces of cells (Figure 2D). Within that apical plane, we demonstrate an asymmetrical distribution of VANGL, which is reflected by a characteristic "chevron-like" pattern iteratively propagated along the length of tubes. These patterns are reminiscent of those observed in flat invertebrate epithelia. Although these observations could be made in large

ducts just prior to birth, observing such patterns in ducts of a smaller diameter presents a challenge, and we are, therefore, unable as yet to ascertain whether planar polarization is established earlier in the pancreatic ductal network. VANGL and other PCP proteins have been shown to control the development of other branching tubular organs, such as the branching of the lungs (Yates et al., 2010b) and the diameter of ducts in the kidney (Yates et al., 2010a; Kunimoto et al., 2017). In the latter, cellular asymmetry of VANGL and FZD protein localization has been inferred from classical 2D sections (Fischer et al., 2006; Karner et al., 2009). In the pancreas, we observed that the apical surface of progenitors lining ducts is anisotropic, with cells being elongated along the duct length. VANGL is enriched at the membrane, delimiting their width rather than their length and more strongly at tricellular junctions, which are known hot-spots of epithelial tension. Their shape is suggestive of a link between PCP component localization and anisotropic stresses in tubes (Higashi and Miller, 2017; Eaton and Jülicher, 2011). As these specialized junctions are involved in cell translocation between epithelial layers and cell intercalation (Higashi and Miller, 2017), an increase of VANGL at the tricellular junctions may affect the egression of endocrine progenitors, thereby coupling morphogenesis and architecture with the endocrine differentiation program. We have shown that inactivation of the PCP components CELRS2/3 leads to a reduced endocrine cell compartment. These components are necessary for PCP function but are not planar polarized. Further work investigating the integrity of the ductal network as well as cellular differentiation in the absence of VANGL protein will be essential to answer whether, like CELRS2/3, it regulates endocrine differentiation, how it exerts this activity and controls ductal cell architecture, and whether it requires a polarized expression to do so.

STAR★METHODS

Detailed methods are provided in the online version of this paper and include the following:

- KEY RESOURCES TABLE
- RESOURCE AVAILABILITY
  - Lead Contact
  - Materials Availability
  - Data and Code Availability
- EXPERIMENTAL MODEL AND SUBJECT DETAILS
- METHOD DETAILS
  - Whole-mount immunohistochemistry
  - Immunohistochemistry on sections
  - Image quantification
  - Gene Expression Analysis
  - Western Blotting
  - Annexin V Apoptosis Assay
  - Pancreatic Bud and Sphere Culture
- QUANTIFICATION AND STATISTICAL ANALYSIS

SUPPLEMENTAL INFORMATION

Supplemental Information can be found online at https://doi.org/10.1016/j.celrep.2020.107677.

ACKNOWLEDGMENTS

We would like to thank M. Figueiredo-Larsen for his experimental contributions with respect to whole-pancreas organoids and Heike Petzold for technical support. We thank D. Devenport for the *Cherry-Vangl2* construct and N. Thompson and the EPFL Transgenesis Core Facility for generating the transgenic lines. We are grateful to J. Bulkescher and G. Karemore for their expert assistance with imaging and statistics, respectively, and to J. Brickman and P. Seymour for their comments on the manuscript. We also thank T. Ohtsuka and J. Nathans for the PK2 and Frizzled3 antibodies, respectively. The Novo Nordisk Foundation Center for Stem Cell Biology is supported by Novo Nordisk Foundation grant number NNF17CC0027852.

AUTHOR CONTRIBUTIONS

L.F. contributed to project design as well as most experimental data collection and analyses; S.Y. contributed to all experiments with the *ex vivo* systems; I.S.B. contributed to the quantification of $CAS3^+$ cells in the *Inversin* mutant and in the neural tube and participated in the analysis of the pancreatosphere videos; C.C. characterized hypoplasia in E16.5 *Cherry-Vangl2* pancreata; M.R.-C.K. quantified pancreatic size in E14.5 *Inversin* mutants; C.C., M.R.-C.K., and L.F. demonstrated VANGL upregulation in *Inversin* mice. A.G.-B. supervised and helped design the project.

DECLARATION OF INTERESTS

C.C. is an employee of Neurimmune. M.R-C.K. is an employee of Société des produits Nestlé SA.

Received: August 16, 2019
Revised: March 31, 2020
Accepted: April 30, 2020
Published: May 26, 2020

REFERENCES

Amonlirdviman, K., Khare, N.A., Tree, D.R., Chen, W.S., Axelrod, J.D., and Tomlin, C.J. (2005). Mathematical modeling of planar cell polarity to understand domineering nonautonomy. Science *307*, 423–426.

Apodaca, G. (2018). Role of Polarity Proteins in the Generation and Organization of Apical Surface Protrusions. Cold Spring Harb. Perspect. Biol. *10*, a027813.

Axelrod, J.D. (2001). Unipolar membrane association of Dishevelled mediates Frizzled planar cell polarity signaling. Genes Dev. *15*, 1182–1187.

Axelrod, J.D., Miller, J.R., Shulman, J.M., Moon, R.T., and Perrimon, N. (1998). Differential recruitment of Dishevelled provides signaling specificity in the planar cell polarity and Wingless signaling pathways. Genes Dev. *12*, 2610–2622.

Bailly, E., Walton, A., and Borg, J.P. (2017). The Planar Cell Polarity Vangl2 protein: from genetics to cellular and molecular functions. Semin. Cell Dev. Biol. *81*, 62–70.

Bankaitis, E.D., Bechard, M.E., and Wright, C.V. (2015). Feedback control of growth, differentiation, and morphogenesis of pancreatic endocrine progenitors in an epithelial plexus niche. Genes Dev. *29*, 2203–2216.

Bastock, R., Strutt, H., and Strutt, D. (2003). Strabismus is asymmetrically localised and binds to Prickle and Dishevelled during Drosophila planar polarity patterning. Development *130*, 3007–3014.

Boutros, M., Paricio, N., Strutt, D.I., and Mlodzik, M. (1998). Dishevelled activates JNK and discriminates between JNK pathways in planar polarity and wingless signaling. Cell *94*, 109–118.

Butler, M.T., and Wallingford, J.B. (2017). Planar cell polarity in development and disease. Nat. Rev. Mol. Cell Biol. *18*, 375–388.

Campanale, J.P., Sun, T.Y., and Montell, D.J. (2017). Development and dynamics of cell polarity at a glance. J. Cell Sci. *130*, 1201–1207.

Carreira-Barbosa, F., Concha, M.L., Takeuchi, M., Ueno, N., Wilson, S.W., and Tada, M. (2003). Prickle 1 regulates cell movements during gastrulation and neuronal migration in zebrafish. Development *130*, 4037–4046.

Chen, H., Mruk, D.D., Lee, W.M., and Cheng, C.Y. (2016). Planar Cell Polarity (PCP) Protein Vangl2 Regulates Ectoplasmic Specialization Dynamics via Its Effects on Actin Microfilaments in the Testes of Male Rats. Endocrinology *157*, 2140–2159.

Chevalier, C., Nicolas, J.F., and Petit, A.C. (2014). Preparation and delivery of 4-hydroxy-tamoxifen for clonal and polyclonal labeling of cells of the surface ectoderm, skin, and hair follicle. Methods Mol. Biol. *1195*, 239–245.

Collombat, P., Hecksher-Sørensen, J., Krull, J., Berger, J., Riedel, D., Herrera, P.L., Serup, P., and Mansouri, A. (2007). Embryonic endocrine pancreas and mature beta cells acquire alpha and PP cell phenotypes upon Arx misexpression. J. Clin. Invest. *117*, 961–970.

Cortijo, C., Gouzi, M., Tissir, F., and Grapin-Botton, A. (2012). Planar cell polarity controls pancreatic beta cell differentiation and glucose homeostasis. Cell Rep. *2*, 1593–1606.

Dahl-Jensen, S.B., Yennek, S., Flasse, L., Larsen, H.L., Sever, D., Karremore, G., Novak, I., Sneppen, K., and Grapin-Botton, A. (2018). Deconstructing the principles of ductal network formation in the pancreas. PLoS Biol. *16*, e2002842.

Daulat, A.M., and Borg, J.P. (2017). Wnt/Planar Cell Polarity Signaling: New Opportunities for Cancer Treatment. Trends Cancer *3*, 113–125.

Devenport, D., and Fuchs, E. (2008). Planar polarization in embryonic epidermis orchestrates global asymmetric morphogenesis of hair follicles. Nat. Cell Biol. *10*, 1257–1268.

Di Gregorio, A., Bowling, S., and Rodriguez, T.A. (2016). Cell Competition and Its Role in the Regulation of Cell Fitness from Development to Cancer. Dev. Cell *38*, 621–634.

Djiane, A., Yogev, S., and Mlodzik, M. (2005). The apical determinants aPKC and dPatj regulate Frizzled-dependent planar cell polarity in the Drosophila eye. Cell *121*, 621–631.

Eaton, S., and Jülicher, F. (2011). Cell flow and tissue polarity patterns. Curr. Opin. Genet. Dev. *21*, 747–752.

Fischer, E., Legue, E., Doyen, A., Nato, F., Nicolas, J.F., Torres, V., Yaniv, M., and Pontoglio, M. (2006). Defective planar cell polarity in polycystic kidney disease. Nat. Genet. *38*, 21–23.

Galea, G.L., Nychyk, O., Mole, M.A., Moulding, D., Savery, D., Nikolopoulou, E., Henderson, D.J., Greene, N.D.E., and Copp, A.J. (2018). Vangl2 disruption alters the biomechanics of late spinal neurulation leading to spina bifida in mouse embryos. Dis. Model. Mech. *11*, dmm032219.

Goodrich, L.V., and Strutt, D. (2011). Principles of planar polarity in animal development. Development *138*, 1877–1892.

Greggio, C., De Franceschi, F., Figueiredo-Larsen, M., Gobaa, S., Ranga, A., Semb, H., Lutolf, M., and Grapin-Botton, A. (2013). Artificial three-dimensional niches deconstruct pancreas development in vitro. Development *140*, 4452–4462.

Greggio, C., De Franceschi, F., Figueiredo-Larsen, M., and Grapin-Botton, A. (2014). In vitro pancreas organogenesis from dispersed mouse embryonic progenitors. J. Vis. Exp. (*89*), 51725.

Habas, R., Kato, Y., and He, X. (2001). Wnt/Frizzled activation of Rho regulates vertebrate gastrulation and requires a novel Formin homology protein Daam1. Cell *107*, 843–854.

Hatakeyama, J., Wald, J.H., Printsev, I., Ho, H.Y., and Carraway, K.L., 3rd. (2014). Vangl1 and Vangl2: planar cell polarity components with a developing role in cancer. Endocr. Relat. Cancer *21*, R345–R356.

Hayes, M.N., Mccarthy, K., Jin, A., Oliveira, M.L., Iyer, S., Garcia, S.P., Sindiri, S., Gryder, B., Motala, Z., Nielsen, G.P., Borg, J.P., Van De Rijn, M., Malkin, D., Khan, J., Ignatius, M.S., and Langenau, D.M. (2018). Vangl2/RhoA Signaling Pathway Regulates Stem Cell Self-Renewal Programs and Growth in Rhabdomyosarcoma. Cell Stem Cell *22*, 414–427.e6.

Higashi, T., and Miller, A.L. (2017). Tricellular junctions: how to build junctions at the TRICkiest points of epithelial cells. Mol. Biol. Cell *28*, 2023–2034.

Hingorani, S.R., Petricoin, E.F., Maitra, A., Rajapakse, V., King, C., Jacobetz, M.A., Ross, S., Conrads, T.P., Veenstra, T.D., Hitt, B.A., et al. (2003). Preinvasive and invasive ductal pancreatic cancer and its early detection in the mouse. Cancer Cell *4*, 437–450.

Iliescu, A., Gravel, M., Horth, C., and Gros, P. (2014). Independent mutations at Arg181 and Arg274 of Vangl proteins that are associated with neural tube defects in humans decrease protein stability and impair membrane targeting. Biochemistry *53*, 5356–5364.

Jenny, A., Darken, R.S., Wilson, P.A., and Mlodzik, M. (2003). Prickle and Strabismus form a functional complex to generate a correct axis during planar cell polarity signaling. EMBO J. *22*, 4409–4420.

Karner, C.M., Chirumamilla, R., Aoki, S., Igarashi, P., Wallingford, J.B., and Carroll, T.J. (2009). Wnt9b signaling regulates planar cell polarity and kidney tubule morphogenesis. Nat. Genet. *41*, 793–799.

Kesavan, G., Sand, F.W., Greiner, T.U., Johansson, J.K., Kobberup, S., Wu, X., Brakebusch, C., and Semb, H. (2009). Cdc42-mediated tubulogenesis controls cell specification. Cell *139*, 791–801.

Knust, E., Tepass, U., and Wodarz, A. (1993). crumbs and stardust, two genes of Drosophila required for the development of epithelial cell polarity. Dev. Suppl. *1993*, 261–268.

Kolahgar, G., Bardet, P.L., Langton, P.F., Alexandre, C., and Vincent, J.P. (2011). Apical deficiency triggers JNK-dependent apoptosis in the embryonic epidermis of Drosophila. Development *138*, 3021–3031.

Kunimoto, K., Bayly, R.D., Vladar, E.K., Vonderfecht, T., Gallagher, A.R., and Axelrod, J.D. (2017). Disruption of Core Planar Cell Polarity Signaling Regulates Renal Tubule Morphogenesis but Is Not Cystogenic. Curr. Biol. *27*, 3120–3131.e4.

Lapébie, P., Borchiellini, C., and Houliston, E. (2011). Dissecting the PCP pathway: one or more pathways?: Does a separate Wnt-Fz-Rho pathway drive morphogenesis? BioEssays *33*, 759–768.

Larsen, H.L., and Grapin-Botton, A. (2017). The molecular and morphogenetic basis of pancreas organogenesis. Semin. Cell Dev. Biol. *66*, 51–68.

Larsen, H.L., Martín-Coll, L., Nielsen, A.V., Wright, C.V.E., Trusina, A., Kim, Y.H., and Grapin-Botton, A. (2017). Stochastic priming and spatial cues orchestrate heterogeneous clonal contribution to mouse pancreas organogenesis. Nat. Commun. *8*, 605.

Lemaire, L.A., Goulley, J., Kim, Y.H., Carat, S., Jacquemin, P., Rougemont, J., Constam, D.B., and Grapin-Botton, A. (2015). Bicaudal C1 promotes pancreatic NEUROG3+ endocrine progenitor differentiation and ductal morphogenesis. Development *142*, 858–870.

Li, D., and Wang, J. (2018). Planar Cell Polarity Signaling in Mammalian Cardiac Morphogenesis. Pediatr. Cardiol. *39*, 1052–1062.

Li, L., Yuan, H., Xie, W., Mao, J., Caruso, A.M., McMahon, A., Sussman, D.J., and Wu, D. (1999). Dishevelled proteins lead to two signaling pathways. Regulation of LEF-1 and c-Jun N-terminal kinase in mammalian cells. J. Biol. Chem. *274*, 129–134.

Lindqvist, M., Horn, Z., Bryja, V., Schulte, G., Papachristou, P., Ajima, R., Dyberg, C., Arenas, E., Yamaguchi, T.P., Lagercrantz, H., and Ringstedt, T. (2010). Vang-like protein 2 and Rac1 interact to regulate adherens junctions. J. Cell Sci. *123*, 472–483.

López-Escobar, B., Caro-Vega, J.M., Vijayraghavan, D.S., Plageman, T.F., Sanchez-Alcazar, J.A., Moreno, R.C., Savery, D., Márquez-Rivas, J., Davidson, L.A., and Ybot-González, P. (2018). The non-canonical Wnt-PCP pathway shapes the mouse caudal neural plate. Development *145*, dev157487.

McGreevy, E.M., Vijayraghavan, D., Davidson, L.A., and Hildebrand, J.D. (2015). Shroom3 functions downstream of planar cell polarity to regulate myosin II distribution and cellular organization during neural tube closure. Biol. Open *4*, 186–196.

Merello, E., Mascelli, S., Raso, A., Piatelli, G., Consales, A., Cama, A., Kibar, Z., Capra, V., and Marco, P.D. (2015). Expanding the mutational spectrum associated to neural tube defects: literature revision and description of novel VANGL1 mutations. Birth Defects Res. A Clin. Mol. Teratol. *103*, 51–61.

Milgrom-Hoffman, M., and Humbert, P.O. (2018). Regulation of cellular and PCP signalling by the Scribble polarity module. Semin. Cell Dev. Biol. *81*, 33–45.

Montcouquiol, M., Rachel, R.A., Lanford, P.J., Copeland, N.G., Jenkins, N.A., and Kelley, M.W. (2003). Identification of Vangl2 and Scrb1 as planar polarity genes in mammals. Nature *423*, 173–177.

Montcouquiol, M., Sans, N., Huss, D., Kach, J., Dickman, J.D., Forge, A., Rachel, R.A., Copeland, N.G., Jenkins, N.A., Bogani, D., et al. (2006). Asymmetric localization of Vangl2 and Fz3 indicate novel mechanisms for planar cell polarity in mammals. J. Neurosci. *26*, 5265–5275.

Moore, M., Marroquin, B.A., Gugliotta, W., Tse, R., and White, S.R. (2004). Rho kinase inhibition initiates apoptosis in human airway epithelial cells. Am. J. Respir. Cell Mol. Biol. *30*, 379–387.

Morgan, D., Turnpenny, L., Goodship, J., Dai, W., Majumder, K., Matthews, L., Gardner, A., Schuster, G., Vien, L., Harrison, W., et al. (1998). Inversin, a novel gene in the vertebrate left-right axis pathway, is partially deleted in the inv mouse. Nat. Genet. *20*, 149–156.

Moriguchi, T., Kawachi, K., Kamakura, S., Masuyama, N., Yamanaka, H., Matsumoto, K., Kikuchi, A., and Nishida, E. (1999). Distinct domains of mouse dishevelled are responsible for the c-Jun N-terminal kinase/stress-activated protein kinase activation and the axis formation in vertebrates. J. Biol. Chem. *274*, 30957–30962.

Müller, H.A., and Wieschaus, E. (1996). armadillo, bazooka, and stardust are critical for early stages in formation of the zonula adherens and maintenance of the polarized blastoderm epithelium in Drosophila. J. Cell Biol. *134*, 149–163.

Narimatsu, M., Bose, R., Pye, M., Zhang, L., Miller, B., Ching, P., Sakuma, R., Luga, V., Roncari, L., Attisano, L., and Wrana, J.L. (2009). Regulation of planar cell polarity by Smurf ubiquitin ligases. Cell *137*, 295–307.

Nishimura, T., Honda, H., and Takeichi, M. (2012). Planar cell polarity links axes of spatial dynamics in neural-tube closure. Cell *149*, 1084–1097.

Norman, M., Wisniewska, K.A., Lawrenson, K., Garcia-Miranda, P., Tada, M., Kajita, M., Mano, H., Ishikawa, S., Ikegawa, M., Shimada, T., and Fujita, Y. (2012). Loss of Scribble causes cell competition in mammalian cells. J. Cell Sci. *125*, 59–66.

Ohsawa, S., Vaughen, J., and Igaki, T. (2018). Cell Extrusion: A Stress-Responsive Force for Good or Evil in Epithelial Homeostasis. Dev. Cell *44*, 532.

Pan, F.C., and Wright, C. (2011). Pancreas organogenesis: from bud to plexus to gland. Dev. Dyn. *240*, 530–565.

Papakrivopoulou, E., Vasilopoulou, E., Lindenmeyer, M.T., Pacheco, S., Brzoska, H.L., Price, K.L., Kolatsi-Joannou, M., White, K.E., Henderson, D.J., Dean, C.H., Cohen, C.D., Salama, A.D., Woolf, A.S., and Long, D.A. (2018). Vangl2, a planar cell polarity molecule, is implicated in irreversible and reversible kidney glomerular injury. J. Pathol. *246*, 485–496.

Park, M., and Moon, R.T. (2002). The planar cell-polarity gene stbm regulates cell behaviour and cell fate in vertebrate embryos. Nat. Cell Biol. *4*, 20–25.

Park, T.J., Gray, R.S., Sato, A., Habas, R., and Wallingford, J.B. (2005). Subcellular localization and signaling properties of dishevelled in developing vertebrate embryos. Curr. Biol. *15*, 1039–1044.

Peng, Y., and Axelrod, J.D. (2012). Asymmetric protein localization in planar cell polarity: mechanisms, puzzles, and challenges. Curr. Top. Dev. Biol. *101*, 33–53.

Román-Fernández, A., and Bryant, D.M. (2016). Complex Polarity: Building Multicellular Tissues Through Apical Membrane Traffic. Traffic *17*, 1244–1261.

Saito, Y., Desai, R.R., and Muthuswamy, S.K. (2018). Reinterpreting polarity and cancer: The changing landscape from tumor suppression to tumor promotion. Biochim. Biophys. Acta Rev. Cancer *1869*, 103–116.

Schindelin, J., Arganda-Carreras, I., Frise, E., Kaynig, V., Longair, M., Pietzsch, T., Preibisch, S., Rueden, C., Saalfeld, S., Schmid, B., et al. (2012). Fiji: an open-source platform for biological-image analysis. Nat. Methods *9*, 676–682.

Schnell, U., and Carroll, T.J. (2016). Planar cell polarity of the kidney. Exp. Cell Res. *343*, 258–266.

Seo, H.S., Habas, R., Chang, C., and Wang, J. (2017). Bimodal regulation of Dishevelled function by Vangl2 during morphogenesis. Hum. Mol. Genet. *26*, 2053–2061.

Shimada, Y., Usui, T., Yanagawa, S., Takeichi, M., and Uemura, T. (2001). Asymmetric colocalization of Flamingo, a seven-pass transmembrane cadherin, and Dishevelled in planar cell polarization. Curr. Biol. *11*, 859–863.

Simons, M., Gloy, J., Ganner, A., Bullerkotte, A., Bashkurov, M., Krönig, C., Schermer, B., Benzing, T., Cabello, O.A., Jenny, A., et al. (2005). Inversin, the gene product mutated in nephronophthisis type II, functions as a molecular switch between Wnt signaling pathways. Nat. Genet. *37*, 537–543.

Street, C.A., and Bryan, B.A. (2011). Rho kinase proteins—pleiotropic modulators of cell survival and apoptosis. Anticancer Res. *31*, 3645–3657.

Strutt, D., and Strutt, H. (2007). Differential activities of the core planar polarity proteins during Drosophila wing patterning. Dev. Biol. *302*, 181–194.

Strutt, H., and Strutt, D. (2008). Differential stability of flamingo protein complexes underlies the establishment of planar polarity. Curr. Biol. *18*, 1555–1564.

Strutt, H., Searle, E., Thomas-Macarthur, V., Brookfield, R., and Strutt, D. (2013). A Cul-3-BTB ubiquitylation pathway regulates junctional levels and asymmetry of core planar polarity proteins. Development *140*, 1693–1702.

Strutt, H., Gamage, J., and Strutt, D. (2016). Robust Asymmetric Localization of Planar Polarity Proteins Is Associated with Organization into Signalosome-like Domains of Variable Stoichiometry. Cell Rep. *17*, 2660–2671.

Sugiyama, T., Benitez, C.M., Ghodasara, A., Liu, L., McLean, G.W., Lee, J., Blauwkamp, T.A., Nusse, R., Wright, C.V., Gu, G., and Kim, S.K. (2013). Reconstituting pancreas development from purified progenitor cells reveals genes essential for islet differentiation. Proc. Natl. Acad. Sci. USA *110*, 12691–12696.

Tao, H., Suzuki, M., Kiyonari, H., Abe, T., Sasaoka, T., and Ueno, N. (2009). Mouse prickle1, the homolog of a PCP gene, is essential for epiblast apical-basal polarity. Proc. Natl. Acad. Sci. USA *106*, 14426–14431.

Tepass, U., Theres, C., and Knust, E. (1990). crumbs encodes an EGF-like protein expressed on apical membranes of Drosophila epithelial cells and required for organization of epithelia. Cell *61*, 787–799.

Torban, E., Iliescu, A., and Gros, P. (2012). An expanding role of Vangl proteins in embryonic development. Curr. Top. Dev. Biol. *101*, 237–261.

Tree, D.R., Shulman, J.M., Rousset, R., Scott, M.P., Gubb, D., and Axelrod, J.D. (2002). Prickle mediates feedback amplification to generate asymmetric planar cell polarity signaling. Cell *109*, 371–381.

Vandenberg, A.L., and Sassoon, D.A. (2009). Non-canonical Wnt signaling regulates cell polarity in female reproductive tract development via van gogh-like 2. Development *136*, 1559–1570.

VanderVorst, K., Hatakeyama, J., Berg, A., Lee, H., and Carraway, K.L., III.. (2018). Cellular and molecular mechanisms underlying planar cell polarity pathway contributions to cancer malignancy. Semin. Cell Dev. Biol. *81*, 78–87.

Vaughen, J., and Igaki, T. (2016). Slit-Robo Repulsive Signaling Extrudes Tumorigenic Cells from Epithelia. Dev. Cell *39*, 683–695.

Ventura, A., Kirsch, D.G., McLaughlin, M.E., Tuveson, D.A., Grimm, J., Lintault, L., Newman, J., Reczek, E.E., Weissleder, R., and Jacks, T. (2007). Restoration of p53 function leads to tumour regression in vivo. Nature *445*, 661–665.

Vicente-Manzanares, M., Ma, X., Adelstein, R.S., and Horwitz, A.R. (2009). Non-muscle myosin II takes centre stage in cell adhesion and migration. Nat. Rev. Mol. Cell Biol. *10*, 778–790.

Villasenor, A., Chong, D.C., Henkemeyer, M., and Cleaver, O. (2010). Epithelial dynamics of pancreatic branching morphogenesis. Development *137*, 4295–4305.

Wald, J.H., Hatakeyama, J., Printsev, I., Cuevas, A., Fry, W.H.D., Saldana, M.J., VanderVorst, K., Rowson-Hodel, A., Angelastro, J.M., Sweeney, C., and Carraway, K.L.R. (2017). Suppression of planar cell polarity signaling and migration in glioblastoma by Nrdp1-mediated Dvl polyubiquitination. Oncogene *36*, 5158–5167.

Wang, Y., Chang, H., Rattner, A., and Nathans, J. (2016). Frizzled Receptors in Development and Disease. Curr. Top. Dev. Biol. *117*, 113–139.

Wu, J., and Mlodzik, M. (2008). The frizzled extracellular domain is a ligand for Van Gogh/Stbm during nonautonomous planar cell polarity signaling. Dev. Cell *15*, 462–469.

Yang, Y., and Mlodzik, M. (2015). Wnt-Frizzled/planar cell polarity signaling: cellular orientation by facing the wind (Wnt). Annu. Rev. Cell Dev. Biol. *31*, 623–646.

Yates, L.L., and Dean, C.H. (2011). Planar polarity: A new player in both lung development and disease. Organogenesis *7*, 209–216.

Yates, L.L., Papakrivopoulou, J., Long, D.A., Goggolidou, P., Connolly, J.O., Woolf, A.S., and Dean, C.H. (2010a). The planar cell polarity gene Vangl2 is required for mammalian kidney-branching morphogenesis and glomerular maturation. Hum. Mol. Genet. *19*, 4663–4676.

Yates, L.L., Schnatwinkel, C., Murdoch, J.N., Bogani, D., Formstone, C.J., Townsend, S., Greenfield, A., Niswander, L.A., and Dean, C.H. (2010b). The PCP genes Celsr1 and Vangl2 are required for normal lung branching morphogenesis. Hum. Mol. Genet. *19*, 2251–2267.

Yokoyama, T., Copeland, N.G., Jenkins, N.A., Montgomery, C.A., Elder, F.F., and Overbeek, P.A. (1993). Reversal of left-right asymmetry: a situs inversus mutation. Science *260*, 679–682.

Yuan, Y., Gao, Y., Wang, H., Ma, X., Ma, D., and Huang, G. (2014). Promoter methylation and expression of the VANGL2 gene in the myocardium of pediatric patients with tetralogy of fallot. Birth Defects Res. A Clin. Mol. Teratol. *100*, 973–984.

STAR★METHODS

KEY RESOURCES TABLE

REAGENT or RESOURCE	SOURCE	IDENTIFIER
Antibodies		
Mouse anti- β-Catenin 1/1000	BD Transduction Labs	Cat# 610153, RRID:AB_397554
Mouse anti- E-Cadherin 1/100	BD Transduction Labs	Cat# 610182, RRID:AB_397581
Rat anti- Cherry 1/1000	Chromotek	Cat# 5f8-100, RRID:AB_2336064
Rabbit anti- Cleaved Caspase-3 1/200	Cell Signaling Technology	Cat# 9664, RRID;AB_2070042
Rabbit anti- Dishevelled2 1/200	Genetex	Cat# GTX103878; RRID:AB_1950156
Rabbit anti- Frizzled3 1/200	Gift from J. Nathans	N/A
chicken anti- GFP 1/1000	Abcam	Cat# ab13970; RRID:AB_300798
guinea pig anti- Glucagon 1/1000	Linco	Cat# 4031-01F, RRID:AB_433707
guinea pig anti- Insulin 1/100	Dako	Cat# A0564, RRID:AB_10013624
hamster anti- Mucin1 1/1000	Thermo Fisher Scientific	Cat# MA5-11202, RRID:AB_11000874
rabbit anti- Par3 1/100	Upstate Millipore	Cat# 07-330; RRID:AB_2101325
rabbit anti- p-cJUN 1/1000	Cell Signaling Technology	Cat# 9164, RRID:AB_330892
goat anti- Pdx1 1/1000	Beta Cell Biology Consortium	Cat# AB2027; RRID:AB_10014625
mouse anti- pHH3 1/100	Cell Signaling Technology	Cat# 9706, RRID:AB_331748
rabbit anti- PKC zeta 1/500	Santa Cruz Biotechnology	Cat# sc-216, RRID:AB_2300359
rabbit anti- pMLC 1/300, 1/1000	Cell Signaling Technology	Cat# 3674, RRID:AB_2147464
rabbit anti- Prickle2 1/1000	Gift from T. Ohtsuka	N/A
goat anti- Scribble 1/100	Santa Cruz Biotechnology	Cat# sc-11049; RRID:AB_2254275
rabbit anti- Sox9 1/500	Chemicon	AB5809
rabbit anti- Sox9* 1/2000	Millipore	Cat# AB5535, RRID:AB_2239761
rat anti- Tubulin 1/10000	Abcam	Cat# ab6160, RRID;AB_305328
rabbit anti- Vangl1/2 1/200, 1/1000	Sigma Aldrich	Cat# HPA025235; RRID:AB_1858718
goat anti- Vangl1/2 1/1000	Santa Cruz Biotechnology	Cat# sc-46561, RRID;AB_2213082
mouse anti- ZO-1 1/200	Thermo Fisher	Cat# 33-9100, RRID:AB_2533147
goat α-chick Al488 1/1000	Thermo Fisher	Cat# A-11039, RRID:AB_2534096
donkey α-goat Al488 1/1000	Abcam	Cat# ab150129; RRID:AB_2687506
donkey α-goat Al488 1/1000	Thermo Fisher	Cat# A-11055; RRID:AB_2534102
goat α-guinea pig Al488 1/2500	Trichem	345-FG-025/CF
goat α-guinea pig Al568 1/800	Thermo Fisher	Cat# A-11075; RRID:AB_2534119
goat α-hamster Al647 1/1000	Jackson Immuno Research	Cat# 127-605-160; RRID:AB_2339001
goat α-hamster Biotinylated 1/500	Jackson Immuno Research	Cat# 127-065-160, RRID:AB_2338980
donkey α-mouse Al488 1/1000	Jackson Immuno Research	Cat# 715-545-150, RRID:AB_2340846
donkey α-mouse Al568 1/1000	Thermo Fisher	Cat# A10037, RRID:AB_2534013
donkey α-mouse Al647 1/800	Jackson Immuno Research	Cat# 715-605-150, RRID:AB_2340862
donkey α-rabbit Biotinylated 1/2000	Thermo Fisher	Cat# A16039, RRID:AB_2534713
donkey α-rabbit HRP 1/400	Jackson Immuno Research	Cat# 711-035-152, RRID:AB_10015282
goat α-rabbit HRP 1/5000	Dako	Cat# P0448, RRID:AB_2617138
donkey α-rabbit Cy3 F(ab¿)2 fragment 1/500	Jackson Immuno Research	Cat# 711-166-152, RRID:AB_2313568
donkey α-rabbit Al647 1/800	Jackson Immuno Research	Cat# 711-605-152, RRID:AB_2492288
donkey α-rat Cy3 1/1000	Jackson Immuno Research	Cat# 712-165-150, RRID:AB_2340666
donkey α-rat Al647 1/500	Jackson Immuno Research	Cat# 712-605-153, RRID:AB_2340694
donkey α-rat Al488 1/5000	Jackson Immuno Research	Cat# 712-545-153, RRID:AB_2340684
donkey α-rat HRP 1/1000	Jackson Immuno Research	Cat# 712-035-153, RRID:AB_2340639

(*Continued on next page*)

Continued

REAGENT or RESOURCE	SOURCE	IDENTIFIER
Critical Commercial Assays		
TSA amplification kit	Perkin Elmer	NEL704A001KT
TSA amplification kit	Molecular probe	T20949
Experimental Models: Organisms/Strains		
Mouse: Gt(ROSA)26Sortm1(cre/ERT2)Tyj/J (Rosa26CreER)	The Jackson Laboratory	MGI:3790674
Mouse: Invs^{Inv}	The Jackson Laboratory	MGI:1856915
Mouse:Tg(Ipf1-cre)1Tuv (Pdx1-Cre)	The Jackson Laboratory	MGI:3032531
Tg (pCAGGS-LoxP-Cherry-Vgl2)AGB	This paper	N/A
Oligonucleotides		
qPCR primer: Vangl2_fw: GGGAGTCGTGGAGATAAATCAG	This paper	N/A
qPCR primer: Vangl2_rv: TTTCTCCCCAGTTGTCATCC	This paper	N/A
Recombinant DNA		
pCAGGS-LoxP-Cherry-Vgl2	This paper	N/A
CMV-CAG-loxP-eGFP-Stop-loxP-IRES-bGal	Collombat et al., 2007	N/A
amino-terminally tagged Cherry–Vangl2	Devenport and Fuchs, 2008	N/A
Software and Algorithms		
Imaris	Bitplane	http://www.bitplane.com/Default.aspx
Fiji	Schindelin et al., 2012	https://imagej.nih.gov/ij/
Prism	GraphPad	https://www.graphpad.com/scientific-software/prism/

RESOURCE AVAILABILITY

Lead Contact

Further information and requests for resources and reagents should be directed to and will be fulfilled by the Lead Contact, Anne Grapin-Botton (botton@mpi-cbg.de)

Materials Availability

Mouse lines generated in this study are available upon request to Lead Contact provided the requestor covers shipping costs.

Data and Code Availability

This study did not generate/analyze datasets or code.

EXPERIMENTAL MODEL AND SUBJECT DETAILS

Mice (*Mus musculus*) of mixed background were housed at the University of Copenhagen with a standard 12 hours light/dark schedule. All experiments were performed according to ethical guidelines approved by the Danish Animal Experiments Inspectorate (Dyreforsøgstilsynet). The following genetically-modified mouse lines were used: *Gt(ROSA)26Sortm1(cre/ERT2)Tyj/J (Rosa26CreER)* (Ventura et al., 2007); *Invs*^{Inv} (Yokoyama et al., 1993) and *Tg(Ipf1-cre)1Tuv (Pdx1-Cre)* (Hingorani et al., 2003). For the *Cherry-Vangl2* lines *(Tg (pCAGGS-LoxP-Cherry-Vgl2)AGB)* the amino-terminally-tagged *Cherry-Vangl2* fusion protein construct (Devenport and Fuchs, 2008) was inserted into a *CMV-CAG-loxP-eGFP-Stop-loxP-IRES-bGal* expression vector (Collombat et al., 2007). We validated by western blot the production of a fusion protein in transfected HEK293T cells (Figure S2M). Three mouse lines (7979, 9140 and 9139) expressing different levels of the transgene were generated by random insertion and the two lines expressing the highest levels of the Cherry-VANGL2 protein (7979 and 9140) were used to collect the data. *Pdx1-Cre*; *Cherry-Vangl2* double-transgenic embryos were obtained by crossing heterozygous *Pdx1-Cre* with heterozygous *Cherry-Vangl2* transgenic mice. After confirming that the single-transgenic embryos did not present any phenotype, we used WT and single-transgenic (*Pdx1-Cre* Tg/+ or *Cherry-Vangl2* Tg/+) littermates indiscriminately as controls. Conditional induction of Cherry-VANGL2 protein was performed by intraperitoneal injection of 4-OH tamoxifen (4-OHTm, Sigma: H6278) at a concentration of 66.6 μg/g in *Rosa26CreER* females mated with *Cherry-Vangl2* males. The 4-OHTm solution was prepared as described previously (Chevalier et al., 2014). For embryo staging, the day of vaginal plug was considered E0.5.,All the embryonic stages used are stated in the main text or in the figure legends. Male and female embryos were used for all the experiments.

METHOD DETAILS

Whole-mount immunohistochemistry

E18.5 or E17.5 dorsal and ventral pancreata together with the first loop of duodenum were dissected and fixed in 4% paraformaldehyde (PFA) in phosphate-buffered saline (PBS) for 2 hours (h) at room temperature (RT) while E14.5 dorsal pancreata were fixed for 30 minutes (min) or 1 h at RT. After washing in PBS and stepwise dehydration in methanol (MeOH), fixed tissue was stored in 100% MeOH at −20°C. To quench autofluorescence, samples were incubated with freshly-prepared MeOH:DMSO:H_2O_2 (2:1:3; 15% H_2O_2) for 12-24 h at RT. Samples were washed twice in 100% MeOH for 30 min at RT. To further permeabilize the tissue, three cycles of incubation at −80°C were performed (1 h at −80°C followed by 1 h at RT). Samples were rehydrated stepwise (15 min per step at RT) in 33%, 66% then 100% TBST (50 mM Tris-HCl pH 7.4, 150 mM NaCl, 0.1% Triton X-100) in MeOH. For VANGL staining, an antigen retrieval step was performed: tissue was immersed in 10 mM trisodium citrate buffer pH 6.0 and heated, at the low pressure setting (106-110°C), to 110°C for 15 min using the TintoRetriever system (BioSB). After blocking for 24 h at 4°C in TNB blocking solution (Perkin Elmer TSA kit: NEL704A001KT) for VANGL staining or in CAS-Block (Thermo Fisher: 8120) for the other stainings, the specimens were incubated with primary antibodies for 48 h at 4°C. Samples were washed extensively in TBST (at least five incubations of 15 min) and incubated with secondary antibodies (for VANGL staining, biotinylated anti-rabbit was used) for 48 h at 4°C. After extensive washes in TBST, a 48 h incubation with Streptavidin-Horse Radish Peroxidase (HRP) (Perkin Elmer TSA kit) was performed to amplify VANGL signal. Other stainings performed in whole-mount did not require any amplification; the samples were therefore dehydrated stepwise to MeOH at this stage. Samples stained with VANGL antibody were washed again in TBST before incubation with Cy3-tyramide for 1 h at RT (Perkin Elmer TSA kit). Then, after washing in TBST, the specimens were dehydrated in MeOH and stored at −20°C. All samples were cleared in a solution of 1:2 benzyl alcohol and benzyl benzoate respectively (BABB) for 12-24 h prior to imaging. Cleared specimens were subsequently mounted in glass concavity slides in BABB. Imaging was performed using a Leica SP8 confocal microscope with a 20x/0.75 IMM CORR objective and hybrid detectors at 1024 × 1024 resolution in an 8-bit format. Three-dimensional reconstructions and movies were performed with Imaris software (Bitplane).

Immunohistochemistry on sections

The whole pancreas and the surrounding organs (duodenum, stomach and spleen) were isolated intact and fixed in 4% PFA in PBS for 30 min (E10.5 and E12.5), 1 h (E14.5) or 2 h (E18.5) at RT. E13.5 and E15.5 samples prepared for DVL2 staining were fixed for 30 min in PFA diluted to 4% in water rather than PBS. After several washes in PBS, samples were equilibrated in 15% sucrose in PBS (0.12 M) solution overnight at 4°C prior to embedding in gelatin (7.5% gelatin diluted in 15% sucrose in PBS 0.12 M solution). Gelatin blocks were subsequently frozen at −65°C in 2-methylbutane (isopentane: Acros Organics) and stored at −80°C until sectioning. Frozen sections (8-10 μm) were then dried at RT and washed in 0.1% Triton X-100 in PBS. The slides were incubated for 10 min in 0.3% Triton X-100 in PBS to permeabilize the tissue. If necessary, an antigen retrieval step was performed at this point (see below). If secondary antibodies directly conjugated to HRP were used, a 7 min incubation in 3% H_2O_2 was performed at this point. The tissues were rinsed and then blocked for 1 h at RT in the appropriate blocking reagent (DVL2 and VANGL, TNB (Perkin Elmer: NEL704A001KT); FZD3, PAR3, PMLC and Scribble, BSA (Molecular probe: T20949); other, CAS-Block (Thermo Fisher: 8120) . Primary antibodies were incubated overnight at 4°C (Key Resources Table). Following three washes in 0.1% Triton X-100 in PBS, the samples were incubated with secondary antibodies for 1 h at RT then rinsed again. For the antibodies requiring amplification (DVL2, VANGL, FZD3, PAR3, PMLC and Scribble) if the secondary antibody was directly conjugated to HRP (FZD3, PAR3, PMLC and Scribble), tyramide labeling was performed using the TSA kit (Molecular Probes: T20949) reagents while, if the secondary antibody was directly conjugated to biotin (DVL2, VANGL), an incubation with streptavidin-HRP of 1 h was performed and followed by Cy3-tyramide labeling (Perkin Elmer TSA kit: NEL704A001KT). For the antibodies that did not require amplification, secondary antibodies directly coupled to Alexa fluor were used, exept for PK2 staining where a secondary α-rabbit Cy3 F(ab′)2 was used (Key Resources Table).The sections were washed extensively before mounting in 80% glycerol in PBS. All images (except those used for quantification, see below) were collected on a Leica SP8 confocal microscope with a 63x/1.30 Glycerol CORR objective and hybrid detectors at 1024 × 1024 resolution in an 8-bit format. Brightness and contrast were adjusted using FIJI software and 3D reconstructions were performed with Imaris software (Bitplane).

Antigen retrieval was performed using the TintoRetriever system (BioSB). The tissue was immersed in 10 mM trisodium citrate buffer pH 6.0 and brought to high temperature for 15 min using either the low pressure setting (106-110°C) or the high pressure setting (114-121°C) depending on the antibody (PK2, VANGL: high pressure; Scribble and PAR3 low pressure) . The samples were gradually equilibrated to RT before proceeding to the next step. For Frizzled3 staining, we used a cycle of 20 min at 95°C.

TUNEL assays were performed with an ApopTag Peroxidase *in situ* apoptosis detection kit (Millipore: S7100) and followed by immunofluorescence staining as described above.

Image quantification

For quantification of the pancreatic epithelium, the entire pancreas was serially sectioned (at 8 μm) and the immunostained sections were imaged using a Leica DM5500 upright wide-field microscope with a 20x air objective. The positive pixels of the section image stained for PDX1, SOX9 or β-catenin/DAPI were quantified on every 8th (E16.5), 6th (E14.5), 5th (E12.5) or every section (E10.5) using a customized Macro in FIJI (Schindelin et al., 2012). The areas obtained for the sampled sections were summed for each pancreas,

providing an estimation of the size of the epithelium. pHH3$^+$, Cleaved Caspase-3$^+$ and TUNEL$^+$ cells (matching a DAPI$^+$ nucleus) were counted manually using Imaris. For each pancreas sample, the ratio between the number of counted cells (pHH3$^+$, Cleaved Caspase-3$^+$ or TUNEL$^+$) and the estimation of the size of the epithelium (based on SOX9$^+$, PDX1$^+$ or β-catenin$^+$/DAPI$^+$ areas) was calculated and then normalized to that for the control littermates.

For the nervous system analysis, the whole embryo was serially sectioned (at 10 μm). After being stained for β-catenin, DAPI and Cleaved Caspase-3, the sections were imaged using a Leica DM5500 upright wide-field microscope with a 20x air objective. Quantifications were made on every 30th section, which corresponds to 10 measurements per embryo. The neural tube was manually segmented based on β-catenin staining using the freehand tool in FIJI. The area of neural tube was then calculated by measuring the positive pixels of β-catenin/DAPI staining included in the hand-traced perimeter using the customized FIJI Macro (Schindelin et al., 2012). Within the area of the neural tube we then calculated the area of Cleaved Caspase-3 signal with the same Macro. For each sample the ratio between the total area of Cleaved Caspase-3 signal/total neural tube area was calculated and normalized to that for control littermates.

Gene Expression Analysis

E14.5 pancreata were lysed in RLT buffer containing 1% β-mercaptoethanol, RNA was purified following the manufacturer's instructions (RNeasy Plus Micro Kit, QIAGEN: 74034) and cDNA was generated by random-primed reverse transcription using SuperScript III reverse transcriptase (Invitrogen: 18080093). Gene expression level was determined by real-time PCR on a StepOnePlus (Applied Biosystems) using Power SYBR Green PCR Master Mix (Applied Biosystems: 4367659). Target gene transcript levels were normalized to Rpl13a expression level (ΔCT). qPCR primers 5′-3′: Vangl2_fw: GGGAGTCGTGGAGATAAATCAG; Vangl2_rv: TTTCTCCCCAGTTGTCATCC

Western Blotting

E12.5 and E15.5 dorsal pancreata were snap-frozen and processed as described (Lemaire et al., 2015) in conjunction with the relevant antibodies (Key Resources Table: p-cJUN 1/1000, pMLC 1/1000, Vangl 1/1000, Tubulin 1/10000). The blots were visualized using a Chemidoc MP (Bio-Rad) and images were quantified based on pixel density using ImageJ. The protein of interest was normalized to alpha tubulin level (internal control) then compared to the average value obtained for control littermates.

Annexin V Apoptosis Assay

E12.5 pancreata were dissected and dissociated with 0.05% trypsin for 10 min at 37°C. The enzymatic reaction was blocked with DMEM/F12 (GIBCO: 10565018) containing 10% fetal bovine serum (GIBCO: 10500064) and cells were washed once in cold PBS. Cells were then washed with annexin-binding buffer and then stained for DAPI (1 μg/ml) and Annexin V following the manufacturer's instructions (Alexa Fluor 647-conjugated anti-Annexin V, diluted 50-fold more than recommended; Invitrogen: A23204). Samples were filtered through a 20 μm strainer and kept on ice, protected from light until FACS analysis. Data were acquired on a BD LSR Fortessa analyzer and analyzed with FCS express 6 (*De Novo* software).

Pancreatic Bud and Sphere Culture

For pancreatic bud culture, E10.5 dorsal pancreatic buds were dissected, the mesenchyme was mechanically removed and the intact epithelium was seeded in 3D Matrigel culture. The buds were cultured in organoid medium (without Y27632) (Greggio et al., 2013) supplemented with either RhoA activator (CN03; Cytoskeleton Inc.), Rock inhibitor (H-1152; Millipore: 555550) or an equal concentration of DMSO for vehicle control. They were cultured for 5 to 7 days and the buds were imaged daily on a AF6000 Leica microscope with a 10x dry objective. In order to determine the working concentration of the compounds, a range of concentrations was initially tested (H1152: 0.25, 0.5, 1, 2.5, 5 and 10 μM; CNO3: 0.25, 0.5 and 1 μg/ml), the buds were collected after treatment and western blotting for pMLC was performed to quantify RhoA/Rock pathway activity. Concentrations of 5 μM H1152 and 1 μg/ml CNO3 were chosen as treatment with these respectively resulted in an average decrease of 68% and an average increase of 133% pMLC protein amount while allowing the epithelium to grow and branch. For the quantifications, the circumference of the growing epithelium was measured using Imaris and exponential growth curves were generated for each bud using GraphPad prism software. The doubling time of each individual growth curve as well as the size of the epithelium at the end point of the culture were used for statistical analysis. Normalization of the data (Figure 6G) was performed for each experimental condition by calculating the ratio (Δ) of the circumference (c) measured at each time-point (t(x)) to the average circumference of the control littermate (C) at the same time-point ($\Delta_{t(x)} = c_{t(x)} / C_{t(x)}$). Δ values were plotted against the time-points of measurement and a linear regression was applied using GraphPad prism software. The slope of each individual line was determined and used for statistical analysis (Figure 6H). Of note, for the sake of clarity, only the average growth curves or the average normalized linear regressions are presented on the graphs for each experimental condition.

For the sphere cultures, E13.5 dorsal pancreata were isolated and the cells were dispersed and seeded in Matrigel as described previously (Greggio et al., 2013, 2014). Spheres were cultured for 4 days prior to live imaging and imaging was performed using either a Leica SP8 confocal microscope with 20x glycerol objective for 5 h (Litter 1: 15 positions imaged for control and 27 positions imaged for *Ch-Vgl2* sample) or using a Zeiss LM780 confocal microscope with 20x dry objective for 3 h (Litter 2: 18 positions imaged for control, 13 for one *Ch-Vgl2* sample and 12 for the second *Ch-Vgl2* sample of the litter). Representative movies were made using FIJI. To

label dead cells, 4-day live spheres were incubated with DAPI (1/1000) for 30 min then washed for 5 min with medium before imaging on a Leica SP8 confocal microscope with 20x glycerol objective.

QUANTIFICATION AND STATISTICAL ANALYSIS

Statistical analyses were performed with GraphPad 6 and Microsoft Excel software. Normalization to control littermates was performed by calculating the ratio between the value obtained for the transgenics (or mutants) and the average value of control littermates, multiplied by 100 to convert to percentages. All statistical tests presented herein are unpaired parametric Student's t tests. P value and number of biological sample can be found in the figure legends. Normality of the data cannot be tested, so is assumed to follow a Gaussian distribution. Results were presented as the mean ± SEM. Fold-change calculations were performed according to the formula: (final value - initial value)/initial value.